

# 1 **Breastmilk-promoted bifidobacteria produce aromatic** 2 **lactic acids in the infant gut**

3  
4 Martin F. Laursen<sup>1#</sup>, Mikiyasu Sakanaka<sup>1,2</sup>, Nicole von Burg<sup>3</sup>, Daniel Andersen<sup>4</sup>, Urs Mörbe<sup>3</sup>,  
5 Aymeric Rivollier<sup>3</sup>, Ceyda T. Pekmez<sup>5</sup>, Janne Marie Moll<sup>4</sup>, Kim F. Michaelsen<sup>5</sup>, Christian  
6 Mølgaard<sup>5</sup>, Mads Vendelbo Lind<sup>5</sup>, Lars O. Dragsted<sup>5</sup>, Takane Katayama<sup>2,6</sup>, Henrik L. Frandsen<sup>1</sup>,  
7 Anne Marie Vinggaard<sup>1</sup>, Martin I. Bahl<sup>1</sup>, Susanne Brix<sup>4</sup>, William Agace<sup>3</sup>, Tine R. Licht<sup>1\*</sup> and  
8 Henrik M. Roager<sup>1,5#\*</sup>

9 # These authors contributed equally

## 10 **Affiliations**

11 <sup>1</sup> National Food Institute, Technical University of Denmark, Kgs. Lyngby, Denmark

12 <sup>2</sup> Faculty of Bioresources and Environmental Sciences, Ishikawa Prefectural University, Ishikawa  
13 921-8836, Japan

14 <sup>3</sup> Department of Health Technology, Technical University of Denmark, Kgs. Lyngby, Denmark

15 <sup>4</sup> Department of Biotechnology and Biomedicine, Technical University of Denmark, Kgs. Lyngby,  
16 Denmark

17 <sup>5</sup> Department of Nutrition, Exercise and Sports, University of Copenhagen, Frederiksberg C,  
18 Denmark

19 <sup>6</sup> Graduate school of Biostudies, Kyoto University, Kyoto 606-8502, Japan

## 20 **Correspondence**

21 \* Tine R. Licht, Tel. + 45 35887186, [trli@food.dtu.dk](mailto:trli@food.dtu.dk), Kemitovet, 2800 Kongens Lyngby,  
22 Denmark

23 \* Henrik M. Roager, Tel. + 45 35324928, [hero@nexs.ku.dk](mailto:hero@nexs.ku.dk), Rolighedsvej 30, 1958 Frederiksberg  
24 C, Denmark

25

## 26 ABSTRACT

27 Breastfeeding profoundly shapes the infant gut microbiota, which is critical for early life immune  
28 development. However, few breastmilk-dependent microbial metabolites mediating host-microbiota  
29 interactions are currently known. We here demonstrate that breastmilk-promoted *Bifidobacterium*  
30 species convert aromatic amino acids (tryptophan, phenylalanine and tyrosine) into their respective  
31 aromatic lactic acids (indolelactate, phenyllactate and 4-hydroxyphenyllactate) via a previously  
32 unrecognised aromatic lactate dehydrogenase. By longitudinal profiling of the gut microbiota  
33 composition and metabolome of stool samples of infants obtained from birth until 6 months of age,  
34 we show that stool concentrations of aromatic lactic acids is determined by the abundance of human  
35 milk oligosaccharide degrading *Bifidobacterium* species containing the aromatic lactate  
36 dehydrogenase. Finally, we demonstrate that stool concentrations of *Bifidobacterium*-derived  
37 indolelactate are associated with the capacity of infant stool samples to activate the aryl  
38 hydrocarbon receptor, a receptor important for maintenance of intestinal homeostasis and immune  
39 system development. These findings open up new directions towards understanding the role of  
40 breastmilk-promoted *Bifidobacterium* in mediating host-microbiota interactions in early life.

## 41 INTRODUCTION

42 Human breastmilk is a perfectly adapted nutritional supply for the infant<sup>1</sup>. Breastfeeding provides  
43 children with important short-term protection against infections, and may also provide long-term  
44 metabolic benefits<sup>1,2</sup>. These benefits may partly be mediated through the gut microbiota, since  
45 breastfeeding is the strongest determinant of gut microbiota composition and function during  
46 infancy<sup>3-5</sup>. Human breastmilk contains human milk oligosaccharides (HMOs), which are complex,  
47 highly abundant sugars serving as substrates for specific microbes including certain species of  
48 *Bifidobacterium*<sup>6</sup>. This co-evolution between bifidobacteria and the host, mediated by HMOs, to a  
49 large extent directs the colonization of the gut in early life, which has critical impact on the immune  
50 system<sup>7</sup>. Depletion of specific microbes, including *Bifidobacterium*, in early life has been associated  
51 with increased risk of allergy and asthma development in childhood<sup>8,9</sup>, and is suggested to  
52 compromise immune function and lead to increased susceptibility to infectious disease<sup>10,11</sup>. Despite  
53 *Bifidobacterium* dominating the gut of breastfed infants and being widely acknowledged as  
54 beneficial, mechanistic insights on the contribution of these bacteria and their metabolites to  
55 immune development during infancy remain limited. Recent studies show that microbial aromatic  
56 amino acid metabolites including tryptophan-derived indoles<sup>12</sup>, via activation of the aryl  
57 hydrocarbon receptor (AhR), can fortify the intestinal barrier<sup>13,14</sup>, protect against pathogenic  
58 infections<sup>15,16</sup> and influence host metabolism<sup>13,17,18</sup>, which makes this group of microbial  
59 metabolites of particular interest in the context of early life.

60 Here, we show that breastmilk-promoted *Bifidobacterium* species, via a previously unrecognised  
61 aromatic lactate dehydrogenase, produce aromatic lactic acids including indolelactate (ILA) in  
62 substantial amounts in the infant gut, and that stool concentrations of this metabolite are associated  
63 with the capacity of infant stool to activate AhR, which is known to impact immune development in  
64 early life.

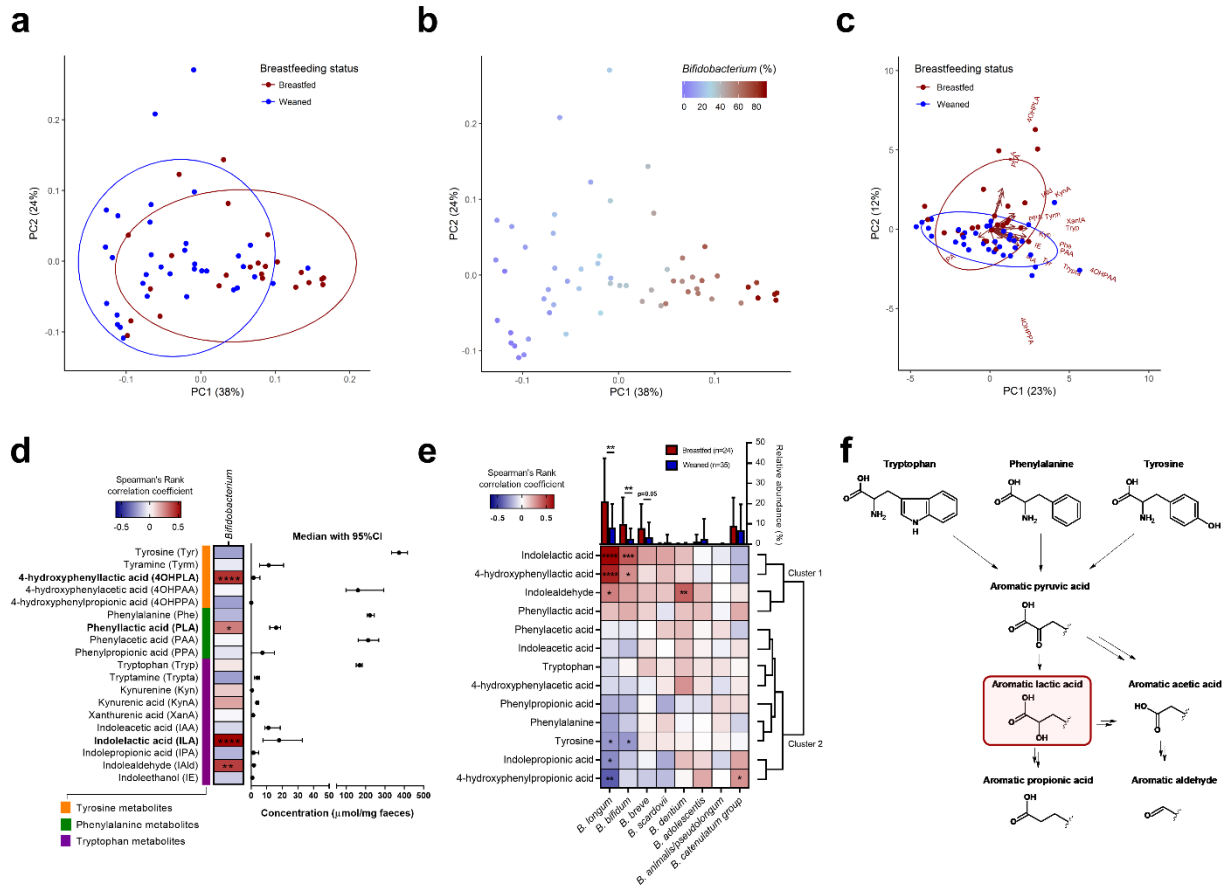
## 65 RESULTS

### 66 *Bifidobacterium* species associate with aromatic amino acid catabolites during late infancy

67 To explore interactions between breastfeeding status, gut microbial composition and metabolism of  
68 aromatic amino acid in early life, we employed 16S rRNA amplicon sequencing to infer gut  
69 microbiota composition and a targeted ultra-performance liquid chromatography mass spectrometry  
70 (UPLC-MS) metabolomics approach to quantify 19 aromatic amino acids and derivatives thereof  
71 (**Supplementary Table 1**) in stool samples from 59 healthy Danish infants from the SKOT I  
72 cohort<sup>19</sup>. The SKOT I infants included were born full term,  $9.1 \pm 0.3$  (mean  $\pm$  SD) months of age at  
73 sampling, and 40.7% were still partially breastfed (**Supplementary Data 1a,b**). After stratification  
74 of the 9 months old infants based on breastfeeding status (partially breastfed versus weaned),  
75 Principal Coordinates Analysis (PCoA) of weighted UniFrac distances showed a significant  
76 separation across the first PC-axis ( $r^2 = 0.093$ ,  $p < 0.001$ , Adonis test; **Fig. 1a**), which was due to an  
77 increasing gradient in relative abundance of *Bifidobacterium* in breastfed infants ( $r^2 = 0.397$ ,  $p <$   
78  $0.001$ , Adonis test; **Fig. 1b**). Other metadata (age, gender, mode of delivery, current formula intake  
79 and age of introduction to solid foods) did not explain gut microbiota variation to the same degree  
80 as breastfeeding status (**Supplementary Data 1c,d**). Principal Component Analysis (PCA) of faecal  
81 aromatic amino acid metabolite concentrations also revealed separation according to breastfeeding  
82 status, which was largely driven by three aromatic lactic acids, 4-hydroxyphenyllactic acid (4-OH-  
83 PLA), phenyllactic acid (PLA) and indolelactic acid (ILA) (**Fig. 1c**). Correlation analysis revealed  
84 that *Bifidobacterium*, but no other bacterial genera, were significantly associated with faecal  
85 concentrations of all three aromatic lactic acids (4-OH-PLA, PLA and ILA), in addition to  
86 indolealdehyde (IAld) (**Fig. 1d** and **Supplementary Data 1e**). *Bifidobacterium* species  
87 (**Supplementary Fig. 1a** and **Supplementary Data 1f**) significantly enriched in the breastfed  
88 infants; *B. longum*, *B. bifidum*, and *B. breve*, were positively associated with the faecal  
89 concentrations of aromatic lactic acids (4-OH-PLA, PLA and ILA) and IAld (cluster 1 in **Fig. 1e**),  
90 but negatively associated with the faecal concentrations of aromatic propionic acids, aromatic  
91 amino acids and to a lesser degree with aromatic acetic acids (cluster 2 in **Fig. 1e**). In contrast, post  
92 weaning type *Bifidobacterium* species, including *B. adolescentis*, *B. animalis/pseudolongum* and *B.*  
93 *catenulatum* group<sup>20,21</sup>, were not significantly associated with aromatic lactic acids nor  
94 breastfeeding status (**Fig. 1e**). These associations were in agreement with the observation that the  
95 concentrations of the three aromatic lactic acids were higher in the faeces of breastfed than in  
96 weaned infants (**Supplementary Fig. 1b**). Furthermore, the abundances of the three aromatic lactic  
97 acids in infant urine (**Supplementary Fig. 2-4**) showed similar positive associations between  
98 relative abundances of breastmilk-promoted *Bifidobacterium* species (**Supplementary Fig. 1c**). In  
99 addition, faecal and urinary levels of ILA were positively correlated ( $\rho = 0.68$ ,  $p < 0.0001$ ),  
100 showing that faecal levels of this metabolite are reflected systemically. Consistently, urine  
101 abundance of ILA, but not of PLA and 4-OH-PLA, were significantly higher in breastfed compared  
102 to weaned infants (**Supplementary Fig. 1b**). Together, this suggests that specific breastmilk-  
103 promoted *Bifidobacterium* species in the gut of infants convert aromatic amino acids to the  
104 corresponding aromatic lactic acids (**Fig. 1f**).

105

106



107

108 **Figure 1. Breastfeeding associates with gut microbiota composition and aromatic amino acid catabolism in 9**  
 109 **months old infants**

110 **a-b**, Principal coordinate analysis plots of weighted UniFrac distances based on OTUs from faecal samples of 9 months  
 111 old infants participating in the SKOT cohort (n = 59). Samples are coloured according to (a) breastfeeding status with  
 112 ellipses indicating 80% CI of data points for partially breastfed (red, n = 24) and weaned (blue, n = 35) infants or (b)  
 113 relative abundance of the genus *Bifidobacterium*.

114 **c**, Principal component analysis plot of concentrations ( $\mu\text{mol}/\text{mg}$  faeces) of aromatic amino acids and their catabolites  
 115 in SKOT faecal samples, coloured according to breastfeeding status with ellipses indicating 80% CI of data points for  
 116 breastfed (red, n = 24) and weaned (blue, n = 35) infants. Loadings are shown with arrows. See abbreviations in (d).

117 **d**, Heatmap illustrating Spearman's Rank correlation coefficients between the relative abundance of *Bifidobacterium*  
 118 and concentrations of aromatic amino acids and their catabolites in SKOT faecal samples (n=59). The concentration of  
 119 each metabolite ( $\mu\text{mol}/\text{mg}$  faeces) is presented as the median with 95% CI.

120 **e**, Heatmap illustrating hierarchical clustering of Spearman's Rank correlation coefficients between the relative  
 121 abundance of the different *Bifidobacterium* species and selected microbial-derived aromatic amino acid catabolites. Bar  
 122 plots are showing relative abundance (mean+SD) of the *Bifidobacterium* spp., stratified according to breastfeeding  
 123 status, with statistical significance evaluated by Mann-Whitney *U* test.

124 **f**, The pathway of aromatic amino acid catabolism by gut microbes (modified from Smith and Macfarlane 1996<sup>95</sup>, Smith  
 125 and Macfarlane 1997<sup>96</sup>, and Zelante *et al.* 2013<sup>16</sup>). Asterisks indicate statistical significance: \*  $p < 0.05$ , \*\*  $p < 0.01$ , \*\*\*  
 126  $p < 0.001$ , \*\*\*\*  $p < 0.0001$ .

127 See also **Supplementary Figure 1-4**.

## 128 ***Bifidobacterium* species produce aromatic lactic acids *in vitro***

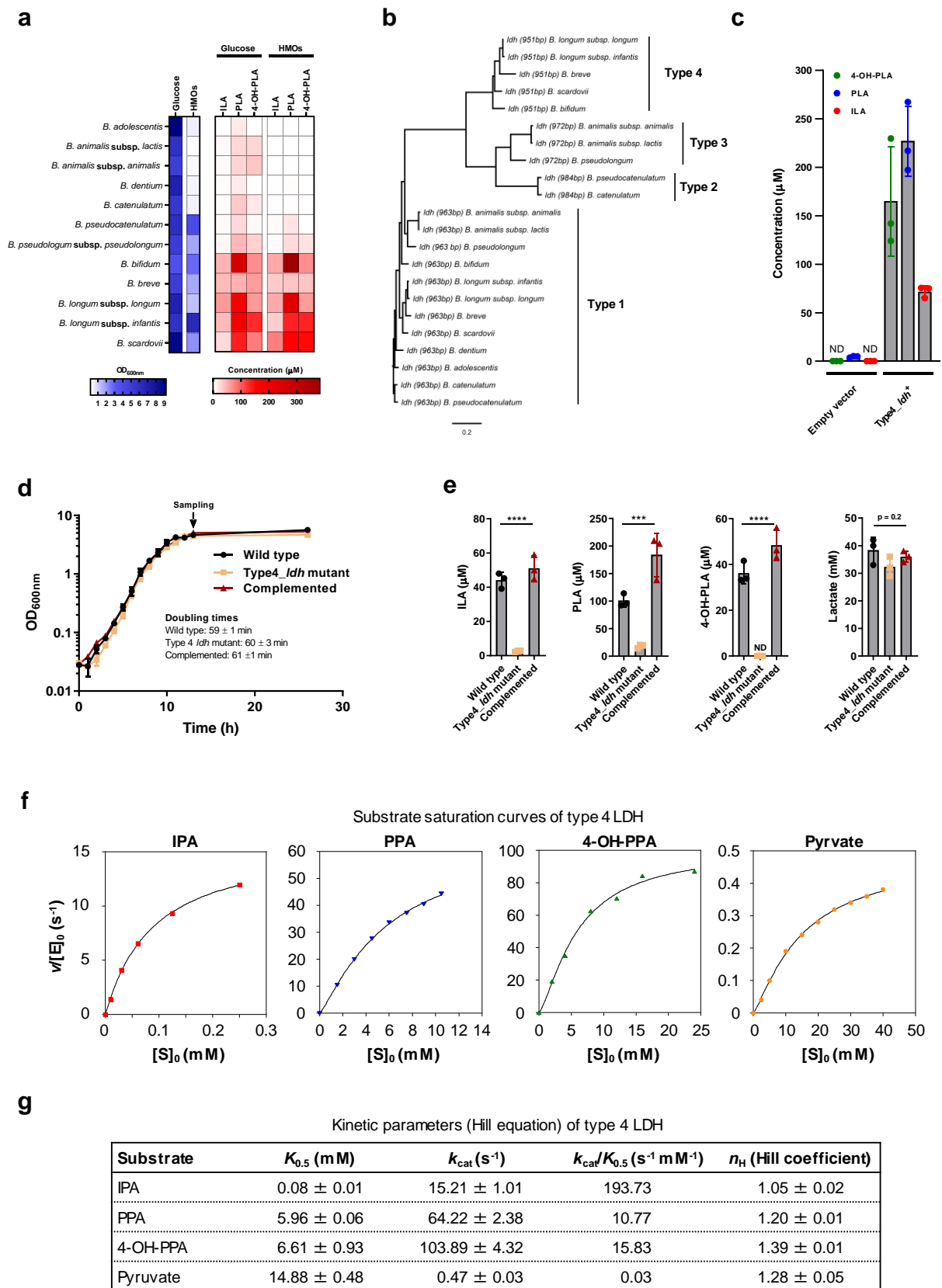
129 To confirm the ability of *Bifidobacterium* species detected in infants to produce aromatic lactic  
130 acids, *Bifidobacterium* type strains were grown anaerobically in a medium containing all three  
131 aromatic amino acids with either glucose or HMOs as sole carbohydrate sources. Analyses of  
132 culture supernatants revealed that ILA, PLA and 4-OH-PLA were produced mainly by *B. bifidum*,  
133 *B. breve*, *B. longum* subsp. *longum*, *B. longum* subsp. *infantis* and *B. scardovii* (**Fig. 2a**), in  
134 accordance with the associations observed in the 9 months old infants (**Fig. 1e**). Other  
135 *Bifidobacterium* species, namely *B. adolescentis*, *B. animalis* subsp. *lactis*, *B. animalis* subsp.  
136 *animalis*, *B. dentium*, *B. catenulatum*, *B. pseudocatenulatum*, *B. pseudolongum* subsp.  
137 *pseudolongum* produced only low amounts of these metabolites (**Fig. 2a**). The ability of  
138 *Bifidobacterium* species to produce high levels of the aromatic lactic acids was generally  
139 convergent with the ability to utilize HMOs as carbohydrate source (**Fig. 2a**), supporting the link  
140 between breastmilk-promoted bifidobacteria and production of aromatic lactic acids. None of the  
141 downstream products of the aromatic lactic acids (**Fig. 1f**) were detected in any of the culture  
142 supernatants.

## 143 **An aromatic lactate dehydrogenase is responsible for the aromatic lactic acid production**

144 Since it has been reported that an L-lactate dehydrogenase (LDH) in *Lactobacillus* spp. can convert  
145 phenylpyruvic acid to PLA<sup>22</sup>, we hypothesized that a corresponding enzyme was present in  
146 *Bifidobacterium* species. Alignment and phylogenetic analysis of all genes annotated as *ldh* in the  
147 *Bifidobacterium* type strains included in this study, revealed four clusters (**Fig. 2b**). Whereas all  
148 *Bifidobacterium* genomes contain an *ldh* responsible for conversion of pyruvate to lactate (here  
149 designated as type 1 *ldh*) in the bifidobacterial fructose-6-phosphate shunt<sup>23,24</sup>, some species have  
150 an extra *ldh*, here designated as type 2, type 3 and type 4, respectively. In agreement with the *in*  
151 *vitro* fermentations (**Fig. 2a**), all prominent aromatic lactic acid-producing *Bifidobacterium* species  
152 contain the type 4 *ldh*. Interestingly, genomic analysis of the *Bifidobacterium* type strains revealed  
153 that the type 4 *ldh* gene is part of a genetic element containing an amino acid transaminase gene  
154 (suspected to be responsible for converting the aromatic amino acids into aromatic pyruvic acids)  
155 and a haloacid dehydrogenase gene (of unknown importance) (**Supplementary Fig. 5**), which has  
156 been indicated to constitute an operon in *B. breve*<sup>25</sup>. Cloning of the type 4 *ldh* gene from *B. longum*  
157 subsp. *infantis*<sup>T</sup> into a vector transformed into *E. coli* revealed that the expression of the type 4 *ldh*  
158 gene indeed resulted in the appearance of PLA, 4-OH-PLA and ILA in the culture supernatant (**Fig.**  
159 **2c**). To verify the type 4 *ldh* dependent production of aromatic lactic acids in *Bifidobacterium*  
160 species, we generated a type 4 *ldh* insertional mutant strain by homologous recombination in *B.*  
161 *longum* subsp. *longum* 105-A (**Supplementary Fig. 6**), a genetically tractable strain containing the  
162 type 4 LDH (**Supplementary Fig. 7**)<sup>26,27</sup>. Cultivation of the wild-type (WT), the type 4 *ldh* mutant  
163 strain and a complemented type 4 *ldh* mutant strain in a medium containing the three aromatic  
164 amino acids (**Supplementary Fig. 6**) confirmed that type 4 *ldh* disruption did not impair growth  
165 (**Fig. 2d**). ILA, PLA and 4-OH-PLA accumulated in the supernatant of the WT and of the  
166 complemented type 4 *ldh* mutant strains, but not in the type 4 *ldh* mutant (**Fig. 2e**). Importantly, the  
167 type 4 *ldh* mutant was not significantly compromised in its ability to convert pyruvate to lactate  
168 (**Fig. 2e**), supporting the distinct role of type 4 *ldh* in converting aromatic pyruvic acids.

169 Purification and characterization of the recombinant type 4 LDH enzyme revealed that it had a mass  
170 of 33.9 kDa (**Supplementary Fig. 8a**), while the native molecular mass was estimated to be 72.9  
171 kDa by size exclusion chromatography, indicating dimer formation in solution (**Supplementary**  
172 **Fig. 8b**). No metal requirement was observed, the optimal pH was 8.0-8.5 and the enzyme was most  
173 stable at 37°C (**Supplementary Fig. 8c-e**). Heterotropic effects were neither observed for  
174 fructose-1,6-bisphosphate (an allosteric effector for type 1 LDH) nor for several intermediates for  
175 aromatic amino acid synthesis<sup>23,24</sup> (**Supplementary Fig. 9**). However, we found that phosphate  
176 served as a positive effector suggesting that type 4 LDH is an intracellular enzyme (**Supplementary**  
177 **Fig. 10a-c**). Assay at the different phosphate concentrations revealed the type 4 LDH is a *K*-type  
178 allosteric enzyme (**Supplementary Fig. 10b,c**). The catalytic rate ( $k_{cat}$ ) was moderate to high for  
179 the aromatic pyruvic acid substrates, but very low for pyruvate (**Fig. 2f,g**), in accordance with the  
180 non-impaired lactate production observed for the type 4 *ldh* mutant (**Fig. 2e**). Production of ILA,  
181 PLA and 4-OH-PLA from the respective aromatic pyruvic acid substrates was verified by high-  
182 performance liquid chromatography (HPLC) (**Supplementary Fig. 10d**). The enzyme showed  
183 highest affinity (lowest  $K_{0.5}$ ) for indole pyruvic acid, but highest catalytic rate for 4-OH-phenyl  
184 pyruvic acid in the presence of 100 mM phosphate (**Fig. 2f,g**). However, maximal catalytic  
185 efficiency ( $k_{cat}/K_{0.5}$ ) was observed for indole pyruvic acid ( $190 \text{ s}^{-1} \text{ mM}^{-1}$ ), followed by 4-OH-phenyl  
186 pyruvic acid ( $16 \text{ s}^{-1} \text{ mM}^{-1}$ ) and phenyl pyruvic acid ( $11 \text{ s}^{-1} \text{ mM}^{-1}$ ), suggesting preference for indole  
187 pyruvic acid. The observed Hill coefficient ( $n_H = 1-1.4$ ) for all substrates indicate weak positive  
188 cooperativity under the conditions tested. Collectively, these results show that the type 4 *ldh* gene  
189 encodes an aromatic lactate dehydrogenase responsible for the production of ILA, PLA and 4-OH-  
190 PLA in *Bifidobacterium* species associated with breastfeeding. We therefore suggest that the type 4  
191 *ldh* gene should be re-classified as an aromatic lactate dehydrogenase gene (*aldh*).

192



193

194 **Figure 2. Bifidobacterium species produce aromatic lactic acids via an aromatic lactate dehydrogenase**  
 195 **a, In vitro production of indolelactic acid (ILA), phenyllactic acid (PLA) and 4-hydroxyphenyllactic acid (4-OH-PLA)**

196 by *Bifidobacterium* spp. type strains in modified MRS medium (MRSc) with 2% (w/v) glucose or a mix human milk  
197 oligosaccharides as sole carbohydrate source. For the type strains of *B. adolescentis*, *B. animalis* subsp. *animalis*, *B.*  
198 *animalis* subsp. *lactis*, *B. dentium* and *B. catenulatum* no or very poor growth ( $OD_{600nm} < 0.4$ ) was observed with HMOs  
199 as carbohydrate source. Mean of three biological replicates is shown.

200 **b**, Neighbor-Joining phylogenetic tree of all genes in the *Bifidobacterium* spp. type strains annotated as L-lactate  
201 dehydrogenases (*ldh*). The four clusters are designated type 1-4.

202 **c**, Production of ILA, PLA and 4-OH-PLA by *E. coli* LMG194 cells transformed with an inducible vector lacking  
203 (empty vector) or containing the type 4 *ldh* (Type4\_ *ldh*<sup>+</sup>) from *B. longum* subsp. *infantis* DSM 20088<sup>T</sup> in LB-medium 5  
204 h post-induction of gene expression by addition of L-arabinose and supplementation with the aromatic pyruvic acids  
205 (indolepyruvate, phenylpyruvate and 4-OH-phenylpyruvate). Bars show mean  $\pm$  SD of three biological replicates.

206 **d**, Growth curves of *Bifidobacterium longum* subsp. *longum* 105-A (wild type), its isogenic insertional type 4 *ldh*  
207 mutant (Type4\_ *ldh* mutant) and the type 4 *ldh* mutant strain complemented with the type 4 *ldh* gene (Complemented).  
208 Curves show mean  $\pm$  SD of three biological replicates and doubling times reported as mean  $\pm$  SD.

209 **e**, Production of ILA, PLA, 4-OH-PLA and lactate by wild type, Type4\_ *ldh* mutant and the complemented strain in  
210 early stationary phase cultures. Bars show mean  $\pm$  SD of three biological replicates. Statistical significance was  
211 evaluated by one-way ANOVA, with \*  $p < 0.05$ , \*\*  $p < 0.01$ , \*\*\*  $p < 0.001$ , \*\*\*\*  $p < 0.0001$ .

212 **f-g**, Enzyme kinetics of the type 4 lactate dehydrogenase. **f**, substrate saturation curves of type 4 LDH with indole  
213 pyruvate, phenylpyruvate, 4-OH-phenylpyruvate or pyruvate as substrates. Data is one representative of two  
214 independent assays. **g**, kinetic parameters of type 4 LDH with the different substrates. Data are mean  $\pm$  SD of two  
215 independent assays.

216 ND, not detected

217 See also **Supplementary Figure 5-10**.

## 218 ***Bifidobacterium* species govern aromatic lactic acid profiles during early infancy**

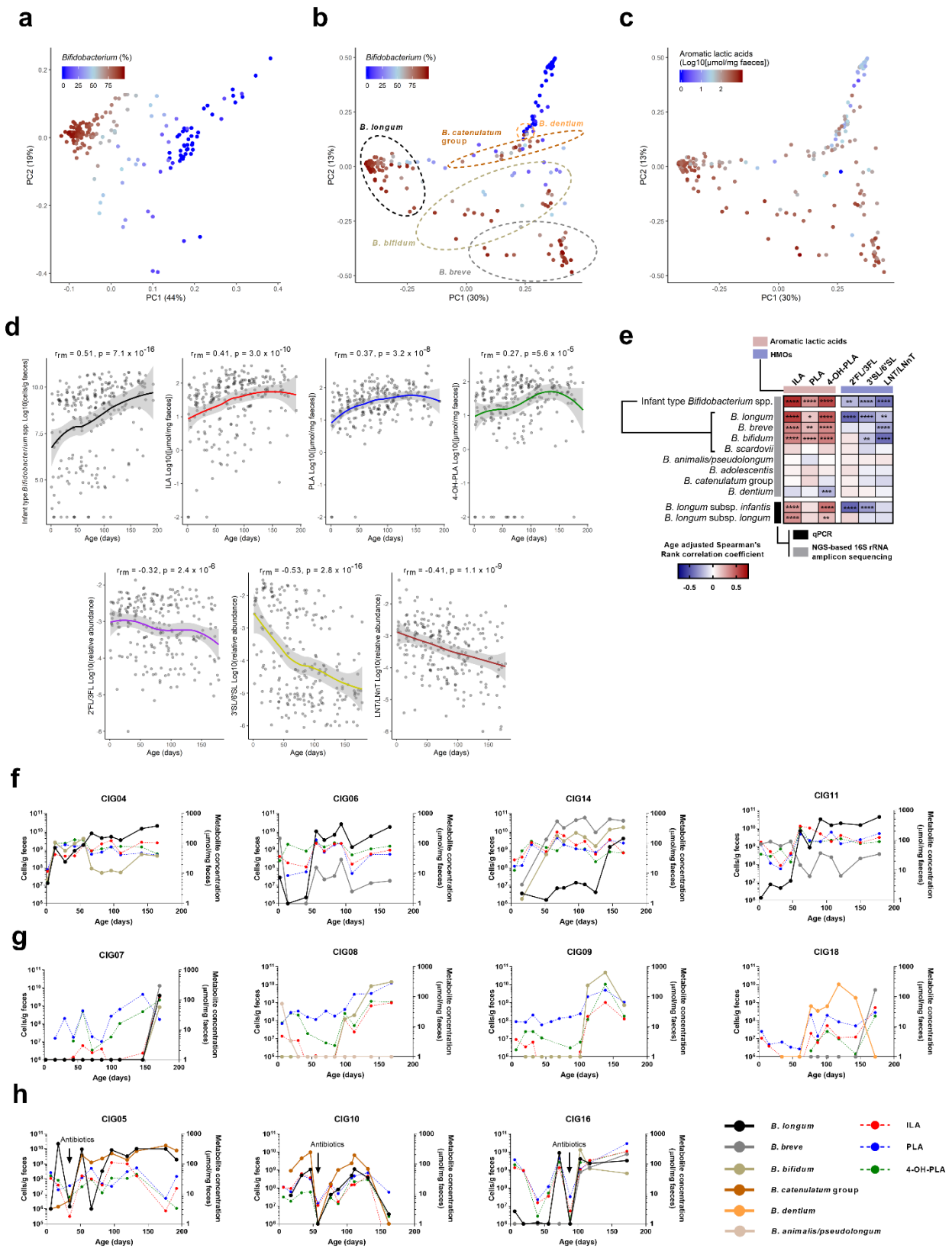
219 To study the dynamics of *Bifidobacterium* species establishment and aromatic lactic acids in  
220 infants, we established the Copenhagen Infant Gut (CIG) cohort including 25 healthy breast- or  
221 mixed fed infants, which were sampled every 2-4 weeks from birth until the age of 6 months  
222 (**Supplementary Data 2a**) for microbiome profiling and targeted metabolite quantification  
223 including aromatic lactic acids (**Supplementary Fig. 11** and **Supplementary Table 2**). A total of  
224 145 operational taxonomic units (OTUs) were detected by 16S rRNA amplicon sequencing,  
225 however, collapsing of OTUs with identical taxonomic classifications and using a cut-off of average  
226 relative abundance of 0.1%, resulted in the identification of 39 bacterial species/taxa, representing  
227 97.5% of the total community (**Supplementary Fig. 11a** and **Supplementary Data 2b**). As  
228 expected, the gut microbiota was highly dominated by *Bifidobacterium* (average of 64.2 %) and  
229 among the top 10 dominating taxa, *B. longum* (38.5 %), *B. breve* (9.1 %), *B. bifidum* (7.9 %), *B.*  
230 *catenulatum* group (6.4 %) and *B. dentium* (1.7 %) were found (**Supplementary Fig. 11a**), with the  
231 remaining *Bifidobacterium* spp. being assigned to *B. scardovii* (0.24 %), *B. adolescentis* (0.15 %)  
232 and *B. animalis/pseudolongum* (0.10 %) (**Supplementary Data 2b,c**). Although the relative  
233 abundance of *Bifidobacterium* increased with time, on average the microbial composition and  
234 Shannon diversity did not change dramatically during the six months (**Supplementary Fig. 11b**).  
235 However, the subject specific gut microbiota profiles revealed a highly individual species  
236 composition (**Supplementary Fig. 11c**) and 48% of the variation in community structure was  
237 explained by subject (weighted UniFrac,  $r^2 = 0.48$ ,  $p < 0.001$ , Adonis, **Supplementary Fig. 12a,b**).  
238 Indeed, the difference in microbial community structure between faecal samples were primarily  
239 driven by the abundance of *Bifidobacterium* as assessed by PCoA of weighted UniFrac distances ( $r^2$



240 = 0.48,  $p < 0.001$ , Adonis, **Fig. 3a**). The non-phylogenetic Bray-Curtis dissimilarity analysis  
241 revealed a separation of the communities based on abundance of the five dominating  
242 *Bifidobacterium* species (*B. longum*, *B. bifidum*, *B. breve*, *B. catenulatum* group and *B. dentium*)  
243 (**Fig. 3b** and **Supplementary Fig. 12c-h**). Community abundance of *B. longum*, *B. bifidum* and *B.*  
244 *breve*, but not *B. catenulatum* group and *B. dentium* (**Fig. 3b**) matched the measured faecal  
245 concentrations of aromatic lactic acids (**Fig. 3c**). Consistently, faecal concentrations of ILA, PLA  
246 and 4-OH-PLA increased concurrently with an increase in absolute abundance of infant type  
247 *Bifidobacterium* species (defined as the summarized abundance of *B. longum*, *B. bifidum*, *B. breve*  
248 and *B. scardovii*) from birth to around 6 months of age (**Fig. 3d, upper panels**). The gut microbiota  
249 of individuals dominated by infant type *Bifidobacterium* spp. was more stable over time than in  
250 individuals with a gut microbiota not dominated by infant type *Bifidobacterium* spp. ( $p < 0.0001$ ,  
251 Mann-Whitney *U* test) (**Supplementary Fig. 12i-j**). Using solely samples from breastfed infants,  
252 faecal abundances of HMO residuals showed a progressive decline with age, concurrent with the  
253 progressive increase in infant type *Bifidobacterium* species (**Fig. 3d, lower panels**). By repeated  
254 measure correlation analyses<sup>28</sup> (**Supplementary Fig. 13**) and partial Spearman's Rank correlation  
255 analyses<sup>29</sup> adjusted for age, we confirmed that the abundance of infant type *Bifidobacterium* species  
256 were positively associated with faecal levels of ILA, PLA and 4-OH-PLA and negatively associated  
257 with abundances of HMOs in faeces (**Fig. 3e**). Both subspecies of *B. longum* were associated with  
258 the aromatic lactic acids, but mainly *B. longum* subsp. *infantis* was associated with the HMO  
259 residuals in faeces (**Fig. 3e**). We have thus established a link between breastfeeding, degradation of  
260 HMOs, abundance of specific infant type *Bifidobacterium* spp. and concentrations of aromatic lactic  
261 acids in early infancy.

262 Examination of the *Bifidobacterium* and aromatic lactic acid dynamics in each of the 25 infants  
263 during the first 6 months of life (**Fig. 3f-h** and **Supplementary Fig. 14-15**) revealed that breastfed  
264 infants early colonised by infant type *Bifidobacterium* species consistently showed high  
265 concentrations of aromatic lactic acids in faeces (**Fig. 3f** and **Supplementary Fig. 15a,b**). In  
266 contrast, infants with delayed infant type *Bifidobacterium* species colonization showed considerably  
267 lower concentrations of the aromatic lactic acids, in particular of ILA, despite breastfeeding (**Fig.**  
268 **3g** and **Supplementary Fig. 15c**). Among the latter, CIG08 and CIG09 were twins, born late  
269 preterm, and dominated by an OTU assigned to *Clostridium neonatale* (**Supplementary Fig. 11c**  
270 and **Supplementary Data 2b**) in accordance with previous reports on *C. neonatale* overgrowth<sup>30</sup>  
271 and delayed *Bifidobacterium* colonization<sup>31-34</sup> in preterm infants. CIG07 who also showed delayed  
272 colonization with infant type *Bifidobacterium*, was mixed fed throughout the whole period and  
273 predominantly colonised with *E. coli* and *Clostridium* spp. (**Supplementary Fig. 11c**). CIG18 had  
274 relatively low faecal concentrations of aromatic lactic acids until age 172 days, when *B. breve*  
275 replaced *B. dentium* (**Fig. 3g**), consistent with the fact that *B. dentium* lacks the *aldh* gene while *B.*  
276 *breve* contains it (**Fig. 2a,b**). Finally, in the three infants treated with antibiotics during our study,  
277 *Bifidobacterium* species abundance were temporarily decreased simultaneously with reduced  
278 concentrations of the aromatic lactic acids (**Fig. 3h**). This indicates that bifidobacterial aromatic  
279 lactic acid production is compromised by pre-term delivery, exposure to antibiotics and formula  
280 supplementation.

281



282

283

284 **Fig. 3. Infant type *Bifidobacterium* species determine aromatic lactic acid concentrations during early infancy**

285 **a-c**, Principal coordinate analysis plots of weighted UniFrac (a) or Bray-Curtis (b-c) distances/dissimilarities (n=234<sup>#</sup>),  
286 coloured according to relative abundance of *Bifidobacterium* (a-b) or log<sub>10</sub> transformed absolute concentration  
287 [µmol/mg faeces] of aromatic lactic acids (sum of indolelactic acid (ILA), phenyllactic acid (PLA) and 4-  
288 hydroxyphenyllactic acid (4-OH-PLA)) in the Copenhagen Infant Gut (CIG) cohort. Dashed lined circles indicate  
289 communities dominated (relative abundance > 50%) either by *B. longum*, *B. bifidum*, *B. breve*, *B. catenulatum* group or  
290 *B. dentium* (*B. adolescentis*, *B. scardovii* and *B. animalis/pseudolongum* never dominated any of the communities, see  
291 **Supplementary Fig 11-12**). <sup>#</sup>6 samples were omitted from the analyses due to low read counts (<8000).

292 **d**, Temporal development in absolute abundance of infant type *Bifidobacterium* spp. (defined as the sum of absolute  
293 abundances of *B. longum*, *B. breve*, *B. bifidum* and *B. scardovii*), faecal concentrations of aromatic lactic acids (ILA,  
294 PLA and 4-OH-PLA, n=240) and relative faecal abundance of HMOs (2'FL/3FL, 2'/3'-O-fucosyllactose; 3'SL/6'SL,  
295 3'/6'-O-sialyllactose; LNT/LNnT, lacto-N-tetraose/ lacto-N-neotetraose, n=228) during the first 6 months of life in the  
296 CIG cohort. A local polynomial regression (LOESS) fit is shown with 95% CI shaded in grey. Statistical significance is  
297 evaluated by repeated measures correlations (r<sub>tm</sub>).

298 **e**, Heatmap illustrating partial Spearman's Rank correlation coefficients (adjusted for age) between the absolute  
299 abundance of *Bifidobacterium* species/subspecies and absolute faecal concentrations of aromatic lactic acids (n=240) or  
300 relative abundances of HMOs (n=228) in the CIG cohort. Infant type *Bifidobacterium* spp. is the sum of absolute  
301 abundances of *B. longum*, *B. breve*, *B. bifidum* and *B. scardovii*. Statistical significance is indicated by asterisks with \*  
302 p<0.05, \*\*p<0.01, \*\*\*p<0.001 and \*\*\*\*p<0.0001.

303 **f-h**, Absolute abundance of *Bifidobacterium* spp. (>1% of total community) and concentrations of ILA, PLA and 4-OH-  
304 PLA in selected individuals from the CIG cohort. **f**, Fully breastfed infants and early colonised with high abundances of  
305 one or more of the infant *Bifidobacterium* spp. (*B. longum*, *B. breve* or *B. bifidum*) and concurrent high absolute  
306 concentrations of ILA, PLA and 4-OH-PLA through the first 6 months of life. **g**, Infants with delayed colonization of  
307 infant type *Bifidobacterium* spp. and concurrent low concentrations of ILA, PLA and 4-OH-PLA. **h**, Infants with  
308 recorded oral antibiotics intake during the first 6 months of life. Similar dynamics of the remaining infants can be seen  
309 in **Supplementary Fig. 15**.

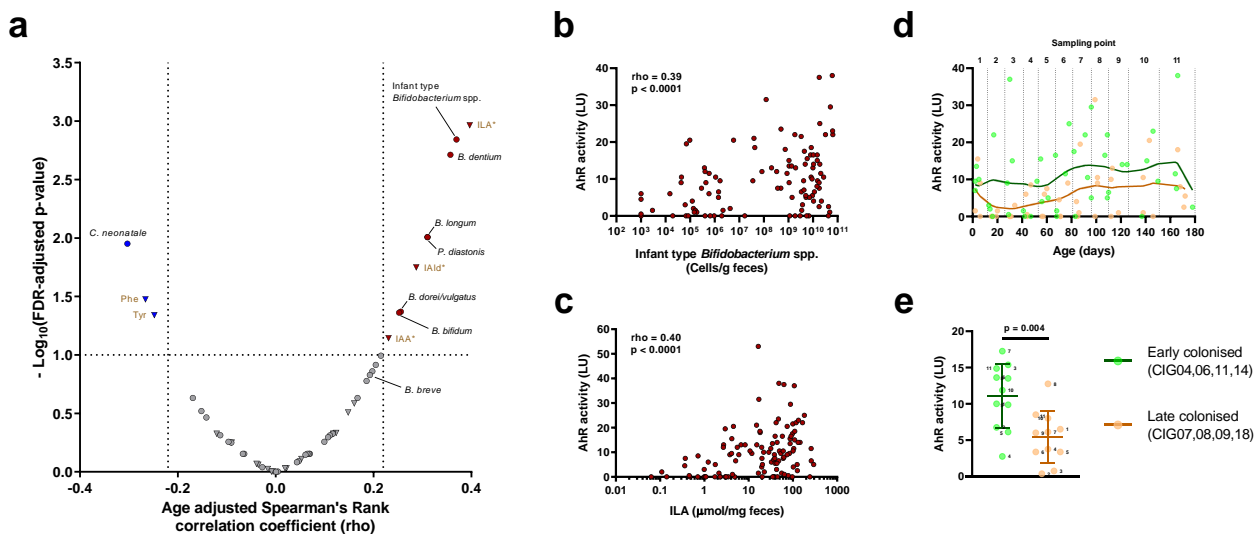
310 **See Supplementary Fig 11-15**

### 311 **Indolelactic acid is a relevant early life AhR agonist**

312 The tryptophan-derived metabolite ILA was the most abundant aromatic lactic acid, as well as the  
313 most abundant tryptophan catabolite measured in the faeces of infants at 0-6 months  
314 (**Supplementary Table 2**) and 9 months of age (**Fig. 1d**). Microbial tryptophan catabolites have  
315 been found to contribute to intestinal and systemic homeostasis, in particular by their ability to bind  
316 the aryl hydrocarbon receptor (AhR)<sup>12</sup>. In accordance with previous reports<sup>16,35</sup>, we observed  
317 modest but significant dose-dependent increases in agonistic activity of ILA in both rat and human  
318 AhR reporter gene cell lines (**Supplementary Fig. 16**). Notably, ILA was more potent in the human  
319 AhR compared to the rat AhR assay (**Supplementary Fig. 16**). To investigate the relationship  
320 between gut microbiota, aromatic amino acid metabolites and AhR signalling, the AhR activity  
321 induced by sterile-filtered faecal water from selected CIG infants (**Fig. 3f-h**) was associated to the  
322 most abundant bacterial taxa and all quantified aromatic amino acid metabolites (n=20) in the same  
323 samples (**Fig. 4a**). This revealed that particularly the infant type *Bifidobacterium* spp. were  
324 positively associated with AhR activity (**Fig. 4b & Supplementary Fig. 17a**). *B. dentium* also  
325 correlated positively with AhR activity despite the absence of an *aldh* gene in this species (**Fig. 4a**),  
326 which might be due to its association to the AhR agonist IAld (**Fig. 1e**), showing similar AhR  
327 reporter activity as ILA (**Supplementary Fig. 16a**). Of all the aromatic amino acid metabolites  
328 measured, only faecal concentrations of three known AhR agonists indoleacetic acid (IAA), IAld  
329 and in particular ILA were significantly associated with AhR activity (**Fig. 4a,c & Supplementary**  
330 **Fig. 17b**). Temporal development in AhR activity was assessed in the CIG samples, and  
331 stratification of infants into those colonised early (**Fig. 3f**) and late (**Fig. 3g**) with infant type  
332 *Bifidobacterium* spp. revealed a higher AhR activity of the faecal water of early colonised infants  
333 (**Fig. 4d-e**). These data show that ILA, produced by *Bifidobacterium* spp. of the infant gut, is a  
334 highly relevant AhR agonist in early life.

335

336



337

338

**Fig. 4. Faecal concentrations of infant type *Bifidobacterium* spp. and indolelactic acid associate with AhR activity**

339

340

341

342

343

344

345

**a**, Scatterplot of age adjusted Spearman's Rank correlation coefficients (versus associated FDR-adjusted p-values) between AhR activity (Luminescence Units, LU) of faecal water (n=119) from selected Copenhagen Infant Gut (CIG) infants (**Fig. 3f-h**, n=11) in a reporter cell line assay and absolute abundance of gut bacterial taxa (relative abundance>0.1%, n=40, circles) or quantities of aromatic amino acid catabolites (n=20, triangles) measured in the same samples. Coloured circles/triangles mark taxa/metabolites measures that are significantly positively (red) or negatively (blue) associated with AhR activity, within an FDR-adjusted p-value of 0.1. Labels are coloured brown for metabolites and black for bacterial taxa. Asterisks indicate known AhR agonists<sup>16</sup>.

346

347

**b-c**, Scatterplots showing the associations from (a) between infant type *Bifidobacterium* spp. (b) or ILA (c) and AhR activity in faecal water from selected CIG infants, assessed by age adjusted Spearman's Rank correlation analysis.

348

349

350

**d**, Temporal development (11 samplings points) of *in vitro* AhR activity in CIG infants early (green; CIG04, CIG06, CIG11 and CIG14) or late (orange; CIG07, CIG08, CIG09, CIG18) colonised with infant type *Bifidobacterium* spp (See **Fig. 3f-g**). Locally weighted regression scatterplot smoothing (LOWESS) curves were fitted to the data points.

351

352

**e**, Scatterplots (mean  $\pm$  SD) of AhR activity for each sampling point, stratifying samples into individuals early and late colonised with infant type *Bifidobacterium*. Statistical significance was evaluated by unpaired *t*-test.

353

See Supplementary Fig 16-17

354

## 355 DISCUSSION

356 The importance of intestinal commensal bacteria in regulation of the intestinal barrier function and  
357 immune development during infancy is well established<sup>36,37</sup>. Yet, specifically the symbiotic role of  
358 the breastmilk-promoted *Bifidobacterium* species, which are highly abundant in breastfed infants,  
359 remains largely unknown. Here we identified an aromatic lactate dehydrogenase, which catalyses  
360 the last step of the conversion of aromatic amino acids into their respective aromatic lactic acids in  
361 the infant gut. We show that only the infant type *Bifidobacterium* species contain the aromatic  
362 lactate dehydrogenase, explaining why *Bifidobacterium* species commonly isolated from the infant  
363 gut *in vitro* produce relative higher levels of ILA compared with other *Bifidobacterium* species<sup>38</sup>.  
364 The infant type *Bifidobacterium* species are adapted to breastfeeding by their HMO-transport and  
365 degradation genes, which provide them with a colonization advantage in infant gut<sup>39-43</sup>. Unlike  
366 HMO-utilization genes, the *aldh* gene appeared not to be important for bifidobacterial proliferation  
367 since disruption of the *aldh* gene did not compromise growth. However, acquisition of *aldh* genes in  
368 breastmilk-promoted *Bifidobacterium* species may provide an evolutionary advantage to the host.  
369 Here, our data suggest that the production of the AhR agonist ILA by breastmilk-promoted  
370 *Bifidobacterium* is a key determinant of AhR-dependent signalling in the gut during infancy.  
371 Indeed, our enzymatic assays show strong adaptation of ALDH towards indolepyruvate, resulting  
372 preferentially in the formation of ILA, the most abundant of the aromatic lactic acids and microbial  
373 tryptophan catabolites detected in our two cohorts. This is potentially of fundamental importance,  
374 since AhR signalling is essential for gut barrier function<sup>44,45</sup> and immune development<sup>15,46-48</sup>.  
375 Microbiota-produced tryptophan-derived AhR ligands (e.g. indolealdehyde) have been shown to  
376 confer colonization resistance against gastrointestinal pathogens<sup>16</sup>, improve intestinal barrier  
377 function<sup>44</sup>, attenuate induced colitis<sup>49</sup> and improve features of metabolic syndrome<sup>44</sup>. Further,  
378 although AhR is conserved across invertebrates and vertebrates, microbiota-derived tryptophan  
379 agonists have shown human-AhR selectivity<sup>50</sup>. In support of this, we found that ILA is a more  
380 potent ligand in the human compared to the rat AhR assay. Considering the strong dominance of  
381 ILA producing *Bifidobacterium* spp. in the gut of breastfed infants, we speculate that ILA provides  
382 an advantage to the infant host by contributing to AhR-mediated early life intestinal and metabolic  
383 homeostasis. A putative mechanism relates to the development of innate lymphoid cells (ILCs),  
384 which are important mediators of innate immunity to bacterial, viral and fungal infections<sup>51</sup>. A  
385 specific subset of ILCs, group 3 ILCs, shows AhR agonist dependency for survival and function  
386 and are reported to be crucial for resistance against gastrointestinal pathogens through the  
387 production of IL-22<sup>16,48</sup>. This effect has been shown to be mediated by microbiota-produced AhR-  
388 agonistic indoles<sup>16</sup>. Thus, we find it plausible that high levels of ILA produced by *Bifidobacterium*  
389 spp. in the infant gut contribute to innate protection against gastrointestinal pathogens. Further, AhR  
390 ligands (including ILA) have been shown to modulate the adaptive immune system by promoting  
391 IL-10+T<sub>reg</sub> induction and suppressing IL-17 and IFN $\gamma$  production by T-cells, potentially reducing  
392 the risk of autoimmunity<sup>52-54</sup>. Non-AhR mediated mechanisms may add to the protective effect, as  
393 ILA and PLA have been shown *in vitro* to have direct anti-bacterial<sup>55,56</sup> and anti-fungal  
394 properties<sup>57,58</sup>. Furthermore, ILA and PLA were recently identified as potent agonists of human  
395 hydroxycarboxylic acid receptor 3 (HCA3)<sup>59</sup>, a receptor expressed in adipocytes, immune cells and  
396 in the intestinal epithelium<sup>60</sup>, involved in the regulation of immune functions and energy

397 homeostasis<sup>61,62</sup>. Thus, the production of aromatic lactic acids by human breastmilk-promoted  
398 *Bifidobacterium* during infancy may represent an evolutionary explanation as to why HCA3 is only  
399 expressed in humans and hominids<sup>59</sup>. In summary, the production of aromatic lactic acids via the  
400 newly identified aromatic lactate dehydrogenase found specifically in breastmilk-promoted species  
401 of *Bifidobacterium* might be an unprecedented feature contributing to intestinal homeostasis and  
402 immune development during infancy. These findings represent a major progress in the  
403 understanding of the beneficial effects of breastmilk, *Bifidobacterium* species and their metabolites  
404 for human health in early life.

## 405 **METHODS**

### 406 **Human study populations and metadata**

#### 407 ***SKOT cohort***

408 The discovery cohort consisted of a random subset of 59 healthy infants of the observational SKOT  
409 I cohort<sup>19</sup>. These infants were originally recruited from Copenhagen and Frederiksberg by random  
410 selection from the National Danish Civil Registry<sup>63</sup>. Inclusion criteria were single birth and full  
411 term delivery, absence of chronic illness and age of 9 months  $\pm$  2 weeks at inclusion. Mode of  
412 delivery, gender, age at sampling, use of medication, breast- and formula feeding prevalence as well  
413 as exclusive and total breastfeeding duration and age of introduction to solid foods was recorded by  
414 parental questionnaires (**Supplementary Data 1a,b**). Anthropometrics, full dietary assessment and  
415 other relevant metadata have been published previously<sup>3,64</sup>. Faecal samples were obtained at 9  
416 months  $\pm$  2 weeks of age and were stored at  $-80^{\circ}\text{C}$  until DNA extraction, as described previously<sup>3</sup>.  
417 Urine samples were collected by the use of cotton balls placed in the infants' disposable nappies  
418 from which the urine was squeezed into a sterile tube and stored at  $-80^{\circ}\text{C}$ . In case of faeces in the  
419 nappy, the urine sample was discarded. The study protocol was approved by the Committees on  
420 Biomedical Research Ethics for the Capital Region of Denmark (H-KF-2007-0003) and The Data  
421 Protection Agency (2002-54-0938, 2007-54-026) approved the study. Informed consent was  
422 obtained from all parents of infants participating in the SKOT I study.

#### 423 ***CIG cohort***

424 The validation cohort, CIG, consisted of 25 healthy infants, vaginally born (23/25) and full-term  
425 (23/25) delivered. Infants in CIG were recruited through social media and limited to the  
426 Copenhagen region. Parents collected faecal samples approximately every second week, starting  
427 from the first week of life until 6 months of age (i.e. within week 0, 2, 4, 6, 8, 10, 12, 16, 20 and  
428 24). Parents were instructed to collect faecal samples from nappies into sterile faeces collection  
429 tubes (Sarstedt, Nümbrecht, Germany) and immediately store them at  $-18^{\circ}\text{C}$  in a home freezer until  
430 transportation to the Technical University of Denmark where the samples were stored at  $-80^{\circ}\text{C}$  until  
431 sample preparation. Gender, pre-term vs full-term birth, mode of delivery, infant/maternal  
432 antibiotics, feeding patterns (breastmilk vs formula), introduction to solid foods and consumption of  
433 probiotics was recorded (**Supplementary Data 2a**). The Data Protection Agency (18/02459)  
434 approved the study. The office of the Committees on Biomedical Research Ethics for the Capital  
435 Region of Denmark confirmed that the CIG study was not notifiable according to the Act on

436 Research Ethics Review of Health Research Projects (Journal nr.: 16049041), as the study only  
437 concerned the faecal microbial composition and activity and not the health of the children. Informed  
438 consent was obtained from all parents of infants participating in the CIG study.

## 439 **Gut microbiota analysis**

### 440 *16S rRNA gene amplicon sequencing*

441 Sample preparation and sequencing was performed as previously described<sup>3</sup> using a subset of 59  
442 faecal samples originating from infants participating in the SKOT I cohort and 241 faecal samples  
443 from 25 infants participating in the CIG cohort (data from a total of 28 samples were missing due to  
444 insufficient DNA extraction, lack of PCR product, very low number of sequencing reads or  
445 resemblance of community to negative controls). Briefly, DNA was extracted from 250 mg faeces  
446 (PowerLyzer® PowerSoil® DNA isolation kit, MoBio 12855-100) and the V3 region of the 16S  
447 rRNA gene was amplified (30s at 98°C, 24-30 cycles of 15s at 98°C and 30s at 72°C, followed by 5  
448 min at 72°C) using non-degenerate universal barcoded primers<sup>65</sup> and then sequenced with the Ion  
449 OneTouch™ and Ion PGM platform with a 318-Chip v2. Sequences from SKOT and CIG were  
450 analyzed separately. Briefly, they were de-multiplexed according to barcode and trimmed as  
451 previously described<sup>65,66</sup> in CLC Genomic Workbench (v8.5. CLCbio, Qiagen, Aarhus, DK).  
452 Quality filtering (-fastq\_filter, MAX\_EE<sub>[SKOT]</sub> = 2.0, MAX\_EE<sub>[CIG]</sub> = 1.0), dereplication, OTU  
453 clustering (-cluster\_otus, minsize 4), chimera filtering (-uchime\_ref, RDP\_gold database), mapping  
454 of reads to OTUs (-usearch\_global, id 97%) and generation of OTU tables (python, uc2otutab.py)  
455 was done according to the UPARSE pipeline<sup>67</sup>. In QIIME<sup>68</sup>, OTU tables (n<sub>OTUs[SKOT]</sub> = 545,  
456 n<sub>OTUs[CIG]</sub> = 478) was filtered to include only OTUs with abundance across all samples above  
457 0.005% of the total OTU counts (n<sub>OTUs[SKOT]</sub> = 258, n<sub>OTUs[CIG]</sub> = 145). OTU relative abundances  
458 within samples were estimated by total sum scaling. Taxonomy was assigned to the OTUs using the  
459 rdp classifier with confidence threshold 0.5<sup>69</sup> and the GreenGenes database v13.8<sup>70</sup>. Estimating  
460 species composition in the CIG cohort, the OTUs detected with identical taxonomy were collapsed  
461 and using a cutoff of average relative abundance of 0.1%, only 39 bacterial species/taxa remained,  
462 representing 97.5% of total community (**Supplementary Data 2b & Supplementary Fig. 11**).  
463 Based on PyNAST alignment of representative OTU sequences from each cohort separately, a  
464 phylogenetic tree was created with FastTree, as described previously<sup>66</sup>. Alpha diversity (Shannon  
465 index, Observed OTUs, Pielou's evenness index) and beta diversity (weighted and unweighted  
466 UniFrac distances, abundance weighted and binary Bray-Curtis and abundance weighted Jaccard  
467 dissimilarities) measures were calculated in QIIME, with the sequencing depth rarefied to 2,000  
468 (SKOT) - 8,000 (CIG) sequences per sample. Jaccard similarity index (1- abundance weighted  
469 Jaccard distance) was computed by calculating the median of all Jaccard similarity index values  
470 between adjacent time points within each individual of the CIG cohort. In order to investigate  
471 *Bifidobacterium* species composition OTUs sequences classified as *Bifidobacterium* according to  
472 the GreenGenes database v13.8 were filtered to remove low abundant OTUs (cutoff 0.1% of total  
473 *Bifidobacterium*) and the taxonomy of these resulting OTUs (n<sub>OTUs[SKOT]</sub> = 23, n<sub>OTUs[CIG]</sub> = 8) was  
474 confirmed by BLAST<sup>71</sup> search against the 16S rRNA gene sequence database at NCBI. The top  
475 BLAST hit indicated species annotation (**Supplementary Data 1f and 2c**). OTUs were collapsed



476 into *Bifidobacterium* species (*B. longum*, *B. bifidum*, *B. breve*, *B. catenulatum* group, *B.*  
477 *adolescentis*, *B. scardovii*, *B. dentium*, *B. animalis/pseudolongum*) based on the top BLAST hit  
478 (**Supplementary Data 1f and 2c**).

#### 479 ***Quantitative PCR***

480 Total bacterial load (universal primers) and absolute abundances of *B. longum* subsp. *longum* and *B.*  
481 *longum* subsp. *infantis* (subspecies specific primers) were estimated by quantitative PCR (qPCR),  
482 using the primers listed in **Supplementary Table 3**. Each reaction was performed (in triplicates)  
483 with 5 µl PCR-grade water, 1.5 µl forward and reverse primer, 10 µl SYBR Green I Master 2X  
484 (LightCycler® 480 SYBR Green I Master, Roche) and 2 µl template DNA, in a total volume of 20  
485 µl. Standard curves were generated from 10-fold serial dilutions of linearized plasmid (containing  
486 10<sup>8</sup> -10<sup>0</sup> gene copies/µl), constructed by cloning a PCR amplified 199bp fragment of the 16S rRNA  
487 gene (V3-region) of *E. coli* (ATCC 25922) or a 307bp fragment of the Blon0915 gene<sup>72</sup> of *B.*  
488 *longum* subsp. *infantis* (DSM 20088) or a 301bp fragment of the BL0274 gene<sup>73</sup> of *B. longum*  
489 subsp. *longum* (DSM 20219) into a pCR4-Blunt-TOPO (Invitrogen) or pCRII-Blunt-TOPO vector  
490 (Invitrogen). Plates were run on the LightCycler® 480 Instrument II (Roche) with the program  
491 including 5 min pre-incubation at 95°C, followed by 45 cycles with 10 sec at 95°C, 15 sec at 50-  
492 60°C and 15 sec at 72°C and a subsequent melting curve analysis including 5 min at 95°C, 1 min at  
493 65°C and continuous temperature increase (ramp rate 0.11 °C/s) until 98°C. Data were analyzed  
494 with the LightCycler® 480 Software (v1.5) (Roche). Bacterial load data (using the universal  
495 primers) were used to estimate absolute abundances of each microbial taxa by multiplying with  
496 relative abundances (derived from 16S rRNA gene amplicon sequencing).

#### 497 ***Bifidobacterium* strains and growth experiments**

##### 498 ***Aromatic lactic acid production by Bifidobacterium type strains***

499 *Bifidobacterium* type strains (**Supplementary Table 4**) were cultivated on MRSc (MRS containing  
500 2% (w/v) glucose and supplemented with 0.05% (w/v) L-cysteine) agar plates for 48h at 37°C  
501 anaerobically. Single colonies were dissolved in 5.0 mL pre-reduced MRSc broth and incubated for  
502 24h at 37°C anaerobically with shake. The overnight cultures were washed (10000xg, room  
503 temperature, 5 min) and resuspended in sterile 0.9% NaCl water, diluted 1:20 (in triplicates) in pre-  
504 reduced MRSc or MRSc+HMOs (MRS broth without glucose, but supplemented with 2.0% (w/v)  
505 HMO mixture and 0.05% (w/v) L-cysteine) and re-incubated at 37°C anaerobically for 72h, after  
506 which OD<sub>600nm</sub> was measured and the culture supernatants (16000xg, 5 min, 4°C) were analysed by  
507 UPLC-MS. The individual HMOs were kindly donated by Glycom A/S (Hørsholm, Denmark); 2'-  
508 *O*-fucosyllactose (2'FL), 3-*O*-fucosyllactose (3FL), lacto-*N*-tetraose (LNT), lacto-*N*-neotetraose  
509 (LNnT), 6'-*O*-sialyllactose (6'SL), 3'-*O*-sialyllactose (3'SL), together representing the three  
510 structures found in human breastmilk (fucosylated, sialylated, and neutral core). Based on the HMO  
511 composition in breastmilk<sup>74,75</sup>, these were mixed in a ratio of 53% 2'FL, 18% 3FL, 13% LNT, 5%  
512 LNnT, 7% 6'SL and 4% 3'SL in sterile water to obtain a representative HMO mix used in the *in*  
513 *vitro* experiments at 2% (w/v).

## 514 **Growth experiment with *B. longum* subsp. *longum* 105-A strains**

515 *B. longum* subsp. *longum* 105-A (JCM 31944) was obtained from Japan Collection of  
516 Microorganisms (RIKEN BioResource Research Center, Tsukuba, Japan). *B. longum* subsp.  
517 *longum* 105-A strains (wild type [WT], insertional mutant [type4 *ldh*::pMSK127] and  
518 complemented insertional mutant [type 4 *ldh*::pMSK127 / pMSK128 (*P<sub>xfp</sub>*-type4 *ldh*)];  
519 **Supplementary Table 4**) were cultivated on MRSc or MRSc-Chl (MRSc supplemented with 2.5  
520 µg/mL chloramphenicol) agar plates for 48h at 37°C anaerobically. Single colonies were dissolved  
521 in 5.4 mL MRSc or MRSc-Chl broth, 10-fold serially diluted and incubated for 15h at 37°C  
522 anaerobically with shake. The most diluted culture (exponential phase) was washed in same  
523 medium (10000xg, room temperature, 5 min) and resuspended in MRSc or MRSc-Chl broth to  
524 yield OD<sub>600nm</sub> = 1 and subsequently diluted 1:40 in prewarmed and reduced MRSc or MRSc-Chl  
525 broth (in triplicates), before incubation at 37°C, anaerobically with shake. The cultures were  
526 sampled (500 µL) every hour for OD<sub>600nm</sub> measurements and the culture supernatants (16000xg,  
527 4°C, 5 min) from early (13h) stationary phase was analyzed by UPLC-MS for aromatic amino  
528 metabolites and by GC-MS for lactate.

## 529 **Alignments and construction of phylogenetic trees**

530 From the full genome sequences (available at <https://www.ncbi.nlm.nih.gov/genome/>) of  
531 *Bifidobacterium* type strains included in this study (**Supplementary Table 4**) all genes annotated as  
532 L-lactate dehydrogenases were aligned (gap cost 10, gap extension cost 1) and subsequently a  
533 phylogenetic tree (Algorithm = Neighbor-Joining, Distance measure = Jukes-Cantor, 100 bootstrap  
534 replications) was constructed in CLC Main Workbench (v7.6.3, CLCbio, Qiagen, Aarhus, DK). The  
535 tree was visualized by use of the FigTree software v1.4.3 (<http://tree.bio.ed.ac.uk/software/figtree/>).  
536 In addition, the type 4 LDH amino acid sequence (translated from the type 4 *ldh* nucleotide  
537 sequence) of *B. longum* subsp. *longum* 105-A was aligned (gap cost 10, gap extension cost 1) with  
538 the type 4 LDH amino acid sequences of the *B. longum* subsp. *longum*, *B. longum* subsp. *infantis*,  
539 *B. bifidum*, *B. breve* and *B. scardovii* type strains. Comparison of type 4 *ldh* gene cluster/operon in  
540 12 *Bifidobacterium* type strains (**Supplementary Fig. 5**) was basically conducted by pairwise  
541 alignments in MBGD (Microbial Genome Database for Comparative Analysis;  
542 <http://mbgd.genome.ad.jp/>). The amino acid sequences of the gene cluster from *B. pseudolongum*  
543 subsp. *pseudolongum* type strain was collected from NCBI database  
544 (<https://www.ncbi.nlm.nih.gov/genome/>) and was used for comparison with that from *B. animalis*  
545 subsp. *animalis* type strain.

## 546 **Recombinant expression of type 4 *ldh***

### 547 ***Chemically competent cells for recombinant expression***

548 *E. coli* LMG 194 ON culture (200µL) was inoculated into 5 ml Luria-Bertani (LB) medium and  
549 incubated at 37°C, 250 rpm until OD<sub>600nm</sub> = 0.5, at which the culture was centrifuged 5 min at  
550 10000xg at 4°C and supernatant discarded. Cell pellet was resuspended in ice-cold 1.8 ml 10mM  
551 MgSO<sub>4</sub> (Sigma, M2643) and centrifuged for 2 min at 5000xg at 0°C. Supernatant was discarded

552 and cell pellet resuspended in 1.8 ml ice-cold 50 mM CaCl<sub>2</sub> (Merck, 1.02083.0250), incubated on  
553 ice for 20 min and centrifuged for 2 min at 5000xg at 0°C. Cell pellet was resuspended in 0.2 ml  
554 ice-cold 100mM CaCl<sub>2</sub>, 10mM MgSO<sub>4</sub> and placed on ice until transformation.

### 555 ***Cloning and recombinant expression***

556 Genomic DNA was extracted (PowerLyzer® PowerSoil® DNA isolation kit, MoBio 12855-100)  
557 from colony material of *B. longum* subsp. *infantis* DSM 20088<sup>T</sup>. In order to amplify the type 4 *ldh*  
558 gene, 50 ng template DNA was mixed with 5 µL 10X PCR buffer, 0.5 µL (50 mM) dNTP mix, 1 µL  
559 (10µM) forward primer (*ldh4\_F*, 5'-ACCATGGTCACTATGAACCG-3'), 1 µL (10µM) reverse  
560 primer (*ldh4\_R*, 5'-AATCACAGCAGCCCCTTG-3') and 1 µL (1 U/µL) Platinum Taq DNA  
561 polymerase (Invitrogen, 10966-018) in a 50 µL total reaction volume. The PCR program included 2  
562 min at 94°C, 35 cycles of 30 sec at 94°C, 30 sec at 55°C, 60 sec at 72°C, followed by a final  
563 extension 10 min at 72°C. The PCR product was purified (MinElute PCR purification kit, Qiagen,  
564 28004) and 4 µL was mixed with 1 µL Salt solution (1.2M NaCl, 0.06M MgCl<sub>2</sub>) and 1 µL pBAD-  
565 TOPO® plasmid (Invitrogen, K4300-01) and incubated for 5 minutes at room temperature. 2 µL of  
566 the cloning mixture was transformed into 50 µL One Shot® TOP10 Competent Cells (Invitrogen,  
567 K4300-01) by gentle mix, incubation 15 min on ice and heat-shock for 30 sec at 42°C. 250µL  
568 S.O.C medium (Invitrogen, K4300-01) was added and incubated at 37°C for 1 h at 200 rpm and  
569 subsequently spread on LB-AMP (LB supplemented with 20 µg/ml Ampicillin (Sigma, A9518))  
570 agar plates and incubated at 37°C ON. Transformants were picked and clean streaked on LB-AMP  
571 agar plates, incubated 37°C, ON and afterwards single colonies of each transformant was inoculated  
572 into 5 ml LB-AMP broth and incubated at 37°C for 15 h at 250 rpm. Plasmid DNA was isolated  
573 (QIAprep Spin Miniprep Kit, Qiagen, 27104) from each transformant and subsequently 5 µL  
574 plasmid DNA (80-100 ng/µL) was mixed with 5µL (5pmol/µL) pBAD forward (5'-  
575 ATGCCATAGCATT TTTTATCC-3') or reverse (5'-GATTTAATCTGTATCAGG-3') sequencing  
576 primers (5pmol/µL) and shipped for sequencing at GATC (GATC-biotech, Koln, Germany). In  
577 order to remove the leader peptide in pBAD-TOPO, 10 µL plasmid (0.1 µg) with correct insert was  
578 cut with FastDigest *NcoI* (Thermo Scientific, FD0563) for 10 min at 37°C and the enzyme  
579 inactivated 15 min at 65°C. Plasmid was ligated using 1 µL (1U/µL) T4 DNA Ligase (Invitrogen,  
580 15224-017) for 5 min at room temperature and subsequently 2µl plasmid was transformed into  
581 100µl chemically competent *E. coli* LMG194 cells by incubation on ice for 30 min, followed by  
582 heat-shock at 43°C for 3 min and incubation on ice for 2 min. 900µL LB medium was added and  
583 cells were incubated at 37°C for 1h at 250 rpm, before plating on LB-AMP agar plates and  
584 incubation at 37°C ON. Transformants were picked, clean streaked and plasmid DNA isolated and  
585 sequenced as described above. A transformant with correct insert was selected for recombinant  
586 expression of the type 4 *ldh* gene; 2 ml LB-AMP broth was inoculated with a single recombinant  
587 colony or the non-transformed *E. coli* LMG194 (negative control) and grown at 37°C ON at  
588 250rpm. In 3x triplicates, 100 µL of the ON cultures (2x3x 100 µL transformant culture + 1x3x 100  
589 µL non-transformed *E. coli* LMG194 culture) were diluted 100-fold into 9.9 mL prewarmed LB-  
590 AMP/LB broth and grown at 37°C, 250 rpm until OD<sub>600nm</sub> ≈ 0.5, at which 9 mL culture was added  
591 1 mL mix of indolepyruvic acid, phenylpyruvic acid and 4-hydroxyphenylpyruvic acid (1mg/mL  
592 each). The cultures were sampled (time zero) and subsequently 100 µL 20% L-arabinose (or 100 uL

593 sterile water; control for induction) was added to induce gene expression and the cultures were re-  
594 incubated at 37°C, 250 rpm, before sampling at 1 h and 5 h post-induction for OD<sub>600nm</sub>  
595 measurements and assessment of production of aromatic lactic acids. For the latter, samples were  
596 centrifuged at 16000xg, 5 min, 4°C and supernatants were stored at -20°C for UPLC-MS analyses.

## 597 **Construction of type 4 *ldh* insertional mutant**

### 598 ***Transformation of B. longum subsp. longum 105-A***

599 *B. longum* subsp. *longum* 105-A cells were grown to exponential phase at 37°C in Gifu anaerobic  
600 liquid medium (Nissui Pharmaceutical Co., Ltd., Tokyo, catalog no. 05422), harvested by  
601 centrifugation, and washed twice with ice-cold 1 mM ammonium citrate buffer containing 50 mM  
602 sucrose (pH = 6.0). The cells were concentrated 200 times with the same buffer and used for  
603 electroporation with settings of 10 kV/cm, 25 µF, and 200Ω. After recovery culturing in Gifu  
604 anaerobic liquid medium at 37°C for 3 h, the cells were spread onto Gifu anaerobic agar containing  
605 antibiotics (i.e. 30 µg/mL spectinomycin and/or 2.5µg/mL chloramphenicol) for selection.

### 606 ***Insertional mutant construction and plasmid complementation***

607 The type 4 *ldh* gene (BL105A\_0985) of *B. longum* subsp. *longum* 105-A was disrupted by a  
608 plasmid-mediated single crossover event as described previously<sup>76</sup>. The plasmid used for disruption  
609 was constructed using the In-Fusion cloning kit (Clontech Laboratories, Inc., Mountain View, CA,  
610 USA, catalog no. 639649). *Escherichia coli* DH5α was used as a host. In brief, the internal region of  
611 the *ldh* gene (position 142-638 of the nucleotide sequence of BL105A\_0985, see **Supplementary**  
612 **Fig. 6**) was amplified by PCR using a primer pair Pr-580/581 (**Supplementary Table 5**) and  
613 ligated with the BamHI-digested pBS423 fragment carrying pUC *ori* and a spectinomycin  
614 resistance gene<sup>26</sup>. The resulting plasmid pMSK127 was introduced into *B. longum* subsp. *longum*  
615 105-A by electroporation to be integrated into type 4 *ldh* locus by single crossover recombination  
616 (type 4 *ldh*::pMSK127). Type 4 *ldh* disruption was confirmed by PCR with a primer pair designed  
617 to anneal outside of the gene (**Supplementary Fig. 6** and **Supplementary Table 5**). The amplified  
618 fragment was also sequenced to ensure the correct recombination event. Complementation plasmid  
619 pMSK128 was constructed by ligating PCR-amplified *xfp* (xylulose 5-phosphate/fructose 6-  
620 phosphate phosphoketolase) promoter region (*P<sub>xfp</sub>*) and the type 4 *ldh* coding region with PstI- and  
621 SalI-digested pBFS38<sup>77</sup> using the In-Fusion cloning kit, by which type 4 *ldh* was placed under the  
622 control of *P<sub>xfp</sub>*. Primer pairs of Pr-598/Pr-599 and Pr-600/Pr-601 were used for amplifying *P<sub>xfp</sub>*  
623 from pBFS48<sup>77</sup> and the type 4 *ldh* gene from the *B. longum* subsp. *longum* 105-A genome,  
624 respectively (**Supplementary Table 5**). The resulting plasmid was electroporated into type 4  
625 *ldh*::pMSK127 to give type 4 *ldh*::pMSK127 / pMSK128 (*P<sub>xfp</sub>*-type4\_ *ldh*) (**Supplementary Fig.**  
626 **6**).

627

## 628 **Biochemical characterization of type 4 LDH**

### 629 *Recombinant expression and purification*

630 Type 4 LDH (BL105A\_0985) was recombinantly expressed as a non-tagged form. The gene was  
631 amplified by PCR using the genomic DNA of *B. longum* subsp. *longum* 105-A as a template and a  
632 primer pair of Pr-617 (5'-GGTGGTGGTGGCTCGAGTCACAGCAGCCCCCTCGCAG-3') and Pr-  
633 635 (5'-AAGGAGATATACATATGGTCACTATGAACCGC-3'). Underlined bases indicate 15-  
634 bp for In-Fusion cloning (Clontech). The amplified DNA fragment was inserted into the NdeI and  
635 XhoI site of pET23b(+) (Novagen) using an In-Fusion HD cloning kit (Clontech). The resulting  
636 plasmid was introduced into *E. coli* BL21 (DE3)  $\Delta lacZ$  carrying pRARE2<sup>76</sup>, and the transformant  
637 was cultured in LB medium supplemented with ampicillin (100  $\mu\text{g ml}^{-1}$ ) and chloramphenicol (7.5  
638  $\mu\text{g ml}^{-1}$ ). When OD<sub>600nm</sub> reached 0.5, isopropyl  $\beta$ -D-thiogalactopyranoside was added at a final  
639 concentration of 0.02 mM to induce the protein expression. The culture was incubated for four days  
640 at 18°C, harvested by centrifugation, and resuspended in 50 mM potassium phosphate buffer (KPB;  
641 pH 7.0) supplemented with 1 mM 2-mercaptoethanol (2-ME) and 200  $\mu\text{M}$  phenylmethane sulfonyl  
642 fluoride. Following cell disruption by sonication, the cleared lysate was saturated with ammonium  
643 sulfate (40–60%). The resulting precipitate was dissolved, dialyzed against 20 mM KPB (pH 7.0)  
644 containing 1 mM 2-ME, and concentrated by Amicon Ultra 10K centrifugal device (Merck  
645 Millipore). The sample was then loaded onto an Affigel blue column (Bio-Rad) preequilibrated with  
646 20 mM KPB (pH 7.0) containing 1 mM 2-ME, and eluted by the same buffer containing 1 M NaCl.  
647 The protein was further purified by a Mono Q 5/50 (GE Healthcare; a linear gradient of 0–1 M  
648 NaCl in 20 mM Tris-HCl (pH 8.0) containing 1 mM 2-ME) and Superdex 200 Increase 10/300 GL  
649 column (GE Healthcare; 10 mM KPB [pH 7.0] containing 50 mM NaCl and 1 mM 2-ME). Protein  
650 concentration was determined by measuring the absorbance at 280 nm based on a theoretical  
651 extinction coefficient of 26,470  $\text{M}^{-1} \text{cm}^{-1}$ .

### 652 *Enzyme assay*

653 The standard reaction mixture contained 100 mM KPB (pH 8.0), 1 mM 2-ME, 0.1 mM  $\beta$ -NADH,  
654 and the substrate. The reaction was initiated by adding the enzyme, and the mixture was incubated  
655 at 37°C for an appropriate time, in which the linearity of the reaction rate was observed. The  
656 substrate concentrations were varied between 0.01 and 0.25 mM for IPA, 1.5 and 12.75 mM for  
657 PPA, 2 and 24 mM for 4-OH-PPA, and 2.5 and 40 mM for pyruvic acid. The enzyme was used at  
658 the concentrations of 0.22 nM for IPA, 1.47 nM for PPA, 0.12 nM for 4-OH-PPA, and 88.50 nM  
659 for pyruvic acid. The reducing reactions of PPA and pyruvic acid was continuously monitored by  
660 measuring the decrease of the absorbance at 340 nm (NADH consumption). When 4-OH-PPA and  
661 IPA were used as the substrates, the reaction products 4-OH-PLA and ILA were quantified by  
662 HPLC after the termination of the reactions by adding 5 % (w/v) trichloroacetic acid. HPLC  
663 analysis was performed using a Waters e2695 separation module (Waters) equipped with a  
664 LiChrospher 100 RP-18 column (250  $\times$  4 mm,  $\phi$  = 5  $\mu\text{m}$ ; Merck Millipore) at 50°C. Following  
665 equilibration with a mixture of 10% solvent A (50% methanol, 0.05% trifluoroacetic acid) and 90%  
666 solvent B (0.05% trifluoroacetic acid) at a flow rate of 1 mL/min, the concentration of solvent A  
667 was linearly increased to 100 % for 25 min and maintained at 100 % for additional 15 min. 4-OH-

668 PLA and ILA were detected by a Waters 2475 Fluorescence Detector with  $\lambda_{\text{ex}}$  277 nm and  $\lambda_{\text{em}}$  301  
669 nm and  $\lambda_{\text{ex}}$  282 nm and  $\lambda_{\text{em}}$  349 nm, respectively. The standard curves were created using the  
670 known concentrations of both compounds. The kinetic parameters ( $k_{\text{cat}}$ ,  $K_{0.5}$ , and Hill coefficient  $n_{\text{H}}$ )  
671 were calculated by curve-fitting the experimental data to the Hill equation, using KaleidaGraph  
672 version 4.1 (Synergy Software). Experiments were performed at least in duplicate. Physicochemical  
673 property of the enzyme was examined by using 1 mM PPA as a substrate. The effects of metal ions  
674 (0.1 mM each) on the enzyme activity was examined using 50 mM MES (2-(*N*-  
675 morpholino)ethanesulfonic acid) buffer (pH 7.0). EDTA (ethylenediaminetetraacetic acid) was  
676 added at the final concentration of 0.1, 0.5, or 1 mM. The optimal pH was determined using 50 mM  
677 KPB (pH 6.0–8.5) and TAPS (*N*-Tris(hydroxymethyl)methyl-3-aminopropanesulfonic acid) buffer  
678 (pH 8.0–9.0). The thermostability was evaluated by the residual activities after incubating the  
679 enzyme (1.0 mg/ml in 10 mM KPB [pH 7.0] containing 50 mM NaCl and 1 mM 2-ME) at the  
680 indicated temperatures for 30 min prior to the assay. Fructose-1,6-bisphosphate, shikimate-3-  
681 phosphate, D-erythrose-4-phosphate, and phosphoenolpyruvate were added to the reaction mixtures  
682 at the concentrations of 0.1 and 1 mM to examine their heterotropic effects. KPB, TAPS buffer, or  
683 HEPES (4-(2-hydroxyethyl)-1-piperazineethanesulfonic acid) buffer (pH 8.0 each) containing 1 and  
684 4 mM PPA as a substrate was used. The effect of phosphate ion was analyzed by adding various  
685 concentration of KPB (pH 8.0) into 10 mM HEPES buffer (pH 8.0). All experiments were  
686 conducted at least in duplicate. In the subsequent kinetic analysis, we used phosphate ion at the  
687 concentration of 100 mM because (i) no saturation was obtained for phosphate under the tested  
688 conditions (**Supplementary Fig. 10a**), (ii) the intracellular phosphate concentration in Gram-  
689 positive bacteria is known to be 130 mM at maximum<sup>78</sup>, and (iii) the strong homotropic effect of  
690 the substrate PPA was observed only in the presence of 10 mM phosphate ion.

## 691 **Metabolomics**

### 692 *Chemicals*

693 Authentic standards of the aromatic amino acids and derivatives (**Supplementary Table 1**) were  
694 obtained from Sigma Aldrich (Germany), whereas isotope-labelled aromatic amino acids used as  
695 internal standards (L-Phenylalanine (ring-d5, 98%), L-Tyrosine (ring-d4, 98%), L-Tryptophan  
696 (indole-d5, 98%) and indoleacetic acid (2,2-d2, 96%)) of the highest purity grade available were  
697 obtained from Cambridge Isotope Laboratories Inc. (Andover, MA).

### 698 *Extraction of metabolites from faecal samples*

699 Faecal samples (100-500 mg) were diluted 1:2 with sterile MQ water, vortexed for 10 seconds and  
700 centrifuged at 16.000xg, 4°C for 5 minutes. Subsequently, the supernatant liquor was transferred to  
701 a new tube and centrifuged again at 16.000xg, 4°C for 10 minutes. Finally, an aliquot of 150-300  
702  $\mu\text{L}$  was stored at -20°C. All samples were later thawed at 4°C, centrifuged at 16.000xg, 4°C for 5  
703 minutes, and diluted in a total volume of 80  $\mu\text{L}$  water corresponding to a 1:5 dilution of the faecal  
704 sample. To each sample, 20  $\mu\text{L}$  internal standard mix (4  $\mu\text{g}/\text{mL}$ ) and 240  $\mu\text{L}$  of acetonitrile were  
705 added. The tubes were vortexed for 10 seconds and left at -20°C for 10 minutes to precipitate the  
706 proteins. The tubes were then centrifuged at 16.000xg, 4°C for 10 minutes and each supernatant

707 (320 µL) was transferred to a new tube, which was dried with nitrogen gas. Subsequently, the  
708 residues were reconstituted in 80 µL water (equalling a 1:5 dilution of the faecal sample with  
709 internal standards having a concentration of 1 µg/mL), vortexed for 10 seconds, centrifuged at  
710 16.000xg, 4°C for 5 minutes, and transferred to LC vial, which was stored at -20°C until analysis.

#### 711 *Extraction of metabolites from urine samples*

712 Urine samples (n=49) from the SKOT cohort were thawed in a refrigerator and all procedures  
713 during the sample preparation were carried out at 0-4°C using an ice bath. The subjects were  
714 randomized between analytical batches by placing all the samples from the each subject in the same  
715 96 well-plate. The run order of the samples was randomized within the analytical batch. Urine  
716 samples were centrifuged at 3000xg for 2 minutes at 4°C. 150 µL of each urine sample were added  
717 to separate wells and diluted with 150 µL of diluent (MQ water: Formic acid (99.9:0.1, v/v) /  
718 Internal standard mixture (100 µg/mL) (90:10, v/v). A blank sample (diluent), standard mixture of  
719 external standard containing 44 biologically relevant metabolites (metabolomics standard)<sup>79</sup> and  
720 pooled sample containing equal amount of each sample (20 µL) were added to spare wells as  
721 quality control samples. The plates were stored at -80°C until the analysis. Immediately prior to  
722 analysis, the plates were thawed and mixed by vortex stirring for 10 minutes.

#### 723 *Extraction of metabolites from in vitro fermentation samples*

724 Supernatants from *in vitro* fermentations were thawed at 4°C, centrifuged at 16.000xg, 4°C for 10  
725 minutes, before 80 µL was transferred to a new tube. To each sample, 20 µL internal standard (40  
726 µg/mL) and 300 µL of acetonitrile were added. The tubes were vortexed for 10 seconds and left at -  
727 20°C for 10 minutes to precipitate the proteins. Following, the tubes were centrifuged at 16.000xg,  
728 4°C for 10 minutes before 50 µL of each sample was diluted with 50 µL of sterile water and  
729 transferred to a LC vial (equalling a 1:10 dilution of the sample with internal standards having a  
730 concentration of 1 µg/mL).

#### 731 *Metabolic profiling of faecal and in vitro samples using UPLC-MS*

732 Aromatic amino acids and derivatives (**Supplementary Table 1**) of faecal and *in vitro* samples  
733 were quantified by ultra performance liquid chromatography mass spectrometry (UPLC-MS) as  
734 previously published<sup>80</sup>.

735 In brief, samples were analysed in random order. For the analysis of the CIG faecal samples, a  
736 pooled quality control (QC) sample was injected for every 10 sample. In all cases, five standard mix  
737 solutions (0.1 µg/mL, 0.5 µg/mL, 1 µg/mL, 2 µg/mL and 4 µg/mL) were analysed once for every 10  
738 samples to obtain a standard curve for every 10 samples. For each sample, a volume of 2 µL was  
739 injected into a ultra-performance liquid chromatography quadrupole time-of-flight mass  
740 spectrometry (UPLC-QTOF-MS) system consisting of Dionex Ultimate 3000 RS liquid  
741 chromatograph (Thermo Scientific, CA, USA) coupled to a Bruker maXis time of flight mass  
742 spectrometer equipped with an electrospray interphase (Bruker Daltonics, Bremen, Germany)  
743 operating in positive mode. The analytes were separated on a Poroshell 120 SB-C18 column with a  
744 dimension of 2.1x100 mm and 2.7 µm particle size (Agilent Technologies, CA, USA) as previously

745 published<sup>80</sup>. Aromatic amino acids and derivatives were detected by selected ions and quantified by  
746 isotopic internal standards with similar molecular structures as listed in **Supplementary Table 1**.  
747 Data were processed using QuantAnalysis version 2.2 (Bruker Daltonics, Bremen, Germany) and  
748 bracket calibration curves for every 10 lumen samples were obtained for each metabolite. The  
749 calibration curves were established by plotting the peak area ratios of all of the analytes with respect  
750 to the internal standard against the concentrations of the calibration standards. The calibration  
751 curves were fitted to a quadratic regression.

752 For untargeted metabolomics, the raw UPLC-MS data, obtained by analysis of the CIG faecal  
753 samples in positive ionization mode, were converted to mzXML files using Bruker Compass  
754 DataAnalysis 4.2 software (Bruker Daltonics) and pre-processed as previously reported<sup>81</sup> using the  
755 R package XCMS (v.1.38.0)<sup>82</sup>. Noise filtering settings included that features should be detected in  
756 minimum 50% of the samples. A data table was generated comprising mass-to charge ( $m/z$ ),  
757 retention time and intensity (peak area) for each feature in the every sample. The data were  
758 normalized to the total intensity. Subsequently, features with a coefficient of variation above 0.3 in  
759 the QC samples and features with a retention time below 0.5 min were excluded from the data.  
760 Parent ion masses of compounds of interest (2'FL/3FL, LNT/LNnT, 3'SL/6'SL) were searched in  
761 the cleaned dataset with 0.02 Da  $m/z$  and 0.02 min retention time tolerance. Subsequently, the  
762 identities of the features of interest were confirmed at level 1<sup>83</sup> by tandem mass spectrometry and  
763 comparison to authentic standards (**Supplementary Table 6**). Of notice, HMO isomers could not  
764 be distinguished with the method applied due to identical retention times.

#### 765 *Metabolic profiling of urine samples using UPLC-MS*

766 The samples were analysed by UPLC coupled with a quadrupole-Time of Flight Mass Spectrometer  
767 (q-TOF-MS) equipped with an electrospray ionization (ESI) (Waters Corporation, Manchester, UK).  
768 Reverse phase HSS T3 C<sub>18</sub> column (2.1x100 mm, 1.8  $\mu$ m) coupled with a pre-column (VanGuard  
769 HSS T3 C<sub>18</sub> column (2.1x5 mm, 1.8  $\mu$ m)) were used for chromatographic separation. Five  $\mu$ l of each  
770 well was injected into the mobile phase A (0.1 % formic acid in MQ water), mobile phase B (10%  
771 1M ammonium acetate in methanol), mobile phase C (methanol) and mobile phase D (isopropanol).  
772 Mobile phase gradient during the run time of 10 min was as follows: start condition (100 % A), 0.75  
773 min (100 % A), 6 min (100 % C), 6.5 min (70 % B, 30 % D), 8 min (70 % B, 30 % D), 8.1 min (70  
774 % B, 30 % D), 9 min (100 % A), 10 min (100 % A). The flow rate gradient was as follows: start  
775 condition (0.4 mL/min), 0.75 min (0.4 mL/min), 6 min (0.5 mL/min), 6.5 min (0.5 mL/min), 8 min  
776 (0.6 mL/min), 8.10 min (0.4 mL/min), 9 min (0.4 mL/min), 10 min (0.4 mL/min). ESI was operated  
777 in negative mode with 3.0 kV capillary probe voltage. The cone voltage and the collision energy were  
778 set at 30 kV and 5 eV, respectively. Ion source and desolvation gas (nitrogen) temperature were 120  
779 and 400 °C while sampling cone and desolvation gas flow rates were 50 and 1000 l/hr. Scan time set  
780 as 0.08 s with 0.02 sec interscan time for both modes. Data were acquired in centroid mode with mass  
781 range between 50 to 1500 Da. Leucine-enkephalin (500 ng/ml) was infused as the lock-spray agent  
782 to calibrate the mass accuracy every 5 sec with 1 sec scan time. Quality control samples were used to  
783 evaluate possible contamination, monitoring the changes in mass accuracy, retention time and  
784 instrumental sensitivity drifts<sup>79,84</sup>.



785 The raw data were converted to netCDF format using DataBridge Software (Waters, Manchester,  
786 UK) and imported into MZmine version 2.28<sup>85</sup>. A subset of samples was used to optimize the pre-  
787 processing parameters for the positive and negative mode data separately. Optimized pre-processing  
788 parameters are listed in **Supplementary Table 7**. Data pre-processing was employed with the  
789 following steps: mass detection, chromatogram builder, chromatogram deconvolution, deisotoping,  
790 peak alignment and gap filling. After the pre-processing, each detected peak was represented by a  
791 feature defined with a retention time,  $m/z$  and peak area.

792 The data matrix was imported into MATLAB R2015b (The MathWorksInc., Natick, MA). Features  
793 that were present in the blanks, were very early and late eluting ( $rt < 0.30$  and  $rt > 9.46$  min), potential  
794 isotopes, duplicates as well as features with masses indicating multiple charges were removed from  
795 the dataset using an in-house algorithm. The data were normalized using unit length normalization to  
796 correct the variation in urine concentration. Parent ion masses of the aromatic lactic acids (ILA, PLA  
797 and 4-OH-PLA) were searched in the cleaned dataset with 0.02 Da  $m/z$  and 0.02 s retention time  
798 tolerance. A linear regression model were employed feature wise to correct for batch differences and  
799 instrumental sensitivity drifts<sup>86</sup>. The aromatic lactic acids were confirmed at level 1<sup>83</sup> by comparison  
800 to authentic standards and by tandem mass spectrometry using the same experimental conditions  
801 (**Supplementary Fig. 2-4**).

#### 802 ***Lactate production by B. longum subsp. longum 105-A strains using GC-MS***

803 The lactate production of the *B. longum* subsp. *longum* 105-A wild-type, type 4 *ldh* mutant and type  
804 4 *ldh* complemented strains were assessed in supernatants obtained after 13h of growth (early  
805 stationary phase) by gas-chromatography mass spectrometry (GC-MS) upon methyl chloroformate  
806 (MCF) derivatisation using a slightly modified version of the protocol previously described<sup>87</sup>. All  
807 samples were analysed in a randomized order. Analysis was performed using GC (7890B, Agilent  
808 Technologies, Inc., Santa Clara, CA) coupled with a quadrupole detector (59977B, Agilent  
809 Technologies, Inc., Santa Clara, CA). The system was controlled by ChemStation (Agilent  
810 Technologies, Inc., Santa Clara, CA). Raw data was converted to netCDF format using  
811 Chemstation, before the data was imported and processed in Matlab R2014b (Mathworks, Inc.)  
812 using the PARADISE software<sup>88</sup>.

#### 813 **Rat Aryl hydrocarbon receptor (AhR) reporter gene assay**

814 Stably transfected rat hepatoma (H4IIE-CALUX) cells provided by Dr. Michael Denison  
815 (University of California, USA) were used. The assay was conducted as previously described<sup>89</sup>,  
816 where cells were incubated for ~22 h in Minimum Essential Medium (MEM) $\alpha$  with 1% foetal  
817 bovine serum (FBS) and 1% penicillin/streptomycin/fungizone. Chemical exposure was performed  
818 for 24 h, and successively luminescence was measured. Cell viability was analyzed by measuring  
819 ATP levels with the CellTiter-Glo<sup>®</sup> Luminescence Assay according to the manufacturer's  
820 instruction (Promega, Denmark). 2,3,7,8-Tetrachlorodibenzo-p-dioxin (TCDD) was used as a  
821 positive control. Three experiments in triplicates were conducted with five 2-fold dilutions of ILA  
822 and IAld ranging from 12.5 to 200  $\mu$ M with a constant vehicle concentration in all wells. Further,  
823 sterile filtered fecal water (10 mg faeces/ml MQ water) obtained from all samples (n=119) of 11

824 selected CIG infants (**Fig. 3f-h**) were run in technical triplicates in the assay. Only mild toxicity that  
825 did not correlate with AhR-luminescence signal was observed for some fecal water samples.

## 826 **Human AhR reporter gene assay**

827 ILA and IAId (positive control)<sup>16</sup> were tested for activation of the human AhR. AhR Reporter Cells  
828 from Indigo Biosciences (PA, USA) that include the luciferase reporter gene functionally linked to  
829 an AhR-responsive promoter were used. The assay was run according to the instructions of the  
830 manufacturer (technical manual version 6.0) with the reference agonist MeBIO as the positive  
831 control. Three experiments in triplicates were conducted with five 2-fold dilutions of ILA and IAId  
832 ranging from 12.5 to 200  $\mu$ M with a constant vehicle concentration in all wells. No cytotoxicity was  
833 observed for any of the tests as determined by a resazurin toxicity assay.

## 834 **Statistical analyses**

835 Statistical analyses were performed using QIIME v1.9<sup>68</sup>, R v3.1<sup>90</sup> and GraphPad Prism v8.1  
836 (GraphPad Software, Inc. CA). PCoA, ADONIS and PERMDISP tests (permutations = 999) of  
837 OTU distance/dissimilarity matrices were performed in QIIME, and PCoA plots were illustrated in  
838 R using the *ggplot2* package<sup>91</sup>. PCA was performed in R using the *ggbiplot* package<sup>92</sup>. Spearman's  
839 Rank correlations were performed in GraphPad Prism, whereas partial Spearman's Rank correlation  
840 analyses with adjustments for age and repeated measures correlation analyses were performed in R  
841 using the *ppcor*<sup>29</sup> and *rmcorr* packages<sup>28</sup>, respectively. Heatmaps and hierarchically clustering of  
842 correlation coefficient were generated in R using the *gplots* package<sup>93</sup> and visualized in GraphPad  
843 Prism. Longitudinal metabolite and taxonomic abundance were modelled using LOESS regression,  
844 and implemented and plotted with 95% confidence intervals in R using the *ggplot2* package<sup>91</sup>.  
845 Longitudinal AhR activity was modelled used coarse LOWESS curve fits within the GraphPad  
846 Prism software. Two-tailed Student's *t* test (if normally distributed, evaluated by D'Agostino-  
847 Pearson test) or two-tailed non-parametric Mann-Whitney *U* test (if not normally distributed) were  
848 performed when comparing two groups. For comparison of more than two groups, statistical  
849 significance was evaluated by one-way ANOVA (if normally distributed) or the non-parametric  
850 Kruskal-Wallis test (if not normally distributed). P-values < 0.05 were considered statistically  
851 significant. When applicable p-values were corrected for multiple testing by the Benjamini-  
852 Hochberg false discovery rate (FDR)<sup>94</sup> using a cutoff of 0.1.

## 853 **ACKNOWLEDGMENTS**

854 We thank the children and families participating in the SKOT I study, which was supported by the  
855 Danish Directorate for Food, Fisheries and Agribusiness (Grant no. 3304-FSE-06-0503), as well as  
856 the children and parents participating in the CIG cohort. Furthermore, we thank Aarstiderne A/S for  
857 providing a small gift for the CIG participants. We thank Marlene Danner Dalgaard at the Technical  
858 University of Denmark in-house facility (DTU Multi-Assay Core, DMAC) for performing the 16S  
859 rRNA gene sequencing, MS-Omics (Hørsholm, Denmark) for performing the lactate analyses,  
860 Glycom A/S (Hørsholm, Denmark) for kindly donating the human milk oligosaccharides, and  
861 Anette Schnipper for her efforts in supporting the work. We also thank Satoru Fukiya and Atsushi

862 Yokota for providing *Bifidobacterium* gene manipulation tools and for technical suggestions, Yuta  
863 Sugiyama for helpful discussions on HPLC analysis, and Shingo Maeda for technical support on  
864 enzyme purification. This work was supported by Augustinus Fonden (grant no. 17-2003 to  
865 H.M.R.), Hørslev Fonden (grant no. 203866 to H.M.R.), Beckett Fonden (grant no. 17-2-0551 to  
866 H.M.R.), Aase og Ejnar Danielsens Fond (grant no. 10-002019 to H.M.R.), the Innovation Fund  
867 Denmark (grant no. 11-116163/0603-00487B; Center for Gut, Grain and Greens to T.R.L.), JSPS-  
868 KAKENHI (18K14379 to M.S., 19K22277 to T.K.), JSPS Overseas Research Fellowships  
869 (201860637 to M.S.) and the Institute for Fermentation, Osaka (to M.S. and T.K.) and “Diet-  
870 induced Arrangement of the gut Microbiome for improvement of Cardiometabolic health“  
871 (DINAMIC) under the Joint Programming Initiative, ”A Healthy Diet for a Healthy Life” (JPI-  
872 HDHL), supported by the Innovation Fund Denmark (grant no. 5195-00001B to L.O.D.).

### 873 **AUTHOR CONTRIBUTIONS**

874 H.M.R. and M.F.L. conceived and designed the experiments. M.F.L. prepared the samples for  
875 sequencing/qPCR and analyzed the sequencing/qPCR data. H.M.R. prepared the samples for faecal  
876 and *in vitro* metabolome analyses and performed together with H.L.F. the targeted and untargeted  
877 metabolomics experiments. C.T.P. and L.O.D. performed the urine metabolomics. M.F.L. and M.S.  
878 performed the *in vitro* growth and mutant construction experiments. M.S. and T.K. performed  
879 enzyme kinetics. K.F.M. and C.M. designed the SKOT I study and M.V.L. managed the data.  
880 H.M.R. and M.F.L. designed the CIG cohort, recruited the study participants and managed the data.  
881 A.M.V. performed the AhR assays. N.B., D.A., U.M., A.R., and J.M.M. contributed to the  
882 interpretation of the results. S.B., W.A., T.K., M.I.B. and T.R.L. contributed with expert  
883 supervision. H.M.R. and M.F.L. led the work, undertook the integrative data analyses and drafted  
884 the manuscript. All authors contributed to and approved the final manuscript.

### 885 **Data statement**

886 Partial (V3 region) 16S rRNA gene amplicon sequencing data is deposited in the Sequence Read  
887 Archive (SRA) under the BioProjects PRJNA273694 (SKOT) and PRJNA554596 (CIG).

### 888 **Competing Financial Interests statement**

889 The authors declare no competing financial interests.

### 890 **Corresponding authors**

891 # Henrik M. Roager

892 # Tine R. Licht

893 **REFERENCES**

- 894 1. Victora, C. G. *et al.* Breastfeeding in the 21st century: epidemiology, mechanisms, and  
895 lifelong effect. *Lancet (London, England)* **387**, 475–90 (2016).
- 896 2. Horta, B. L., Loret de Mola, C. & Victora, C. G. Long-term consequences of breastfeeding  
897 on cholesterol, obesity, systolic blood pressure and type 2 diabetes: a systematic review and  
898 meta-analysis. *Acta Paediatr.* **104**, 30–7 (2015).
- 899 3. Laursen, M. F. *et al.* Infant Gut Microbiota Development Is Driven by Transition to Family  
900 Foods Independent of Maternal Obesity. *mSphere* **1**, e00069-15 (2016).
- 901 4. Bäckhed, F. *et al.* Dynamics and stabilization of the human gut microbiome during the first  
902 year of life. *Cell Host Microbe* **17**, 690–703 (2015).
- 903 5. Stewart, C. J. *et al.* Temporal development of the gut microbiome in early childhood from  
904 the TEDDY study. *Nature* **562**, 583–588 (2018).
- 905 6. Bode, L. The functional biology of human milk oligosaccharides. *Early Hum. Dev.* **91**, 619–  
906 622 (2015).
- 907 7. Gensollen, T., Iyer, S. S., Kasper, D. L. & Blumberg, R. S. How colonization by microbiota  
908 in early life shapes the immune system. *Science (80-. )*. **352**, 539–544 (2016).
- 909 8. Stokholm, J. *et al.* Maturation of the gut microbiome and risk of asthma in childhood. *Nat.*  
910 *Commun.* **9**, 141 (2018).
- 911 9. Fujimura, K. E. *et al.* Neonatal gut microbiota associates with childhood multisensitized  
912 atopy and T cell differentiation. *Nat. Med.* **22**, 1187–1191 (2016).
- 913 10. Khosravi, A. & Mazmanian, S. K. Disruption of the gut microbiome as a risk factor for  
914 microbial infections. *Curr. Opin. Microbiol.* **16**, 221–227 (2013).
- 915 11. Fukuda, S. *et al.* Bifidobacteria can protect from enteropathogenic infection through  
916 production of acetate. *Nature* **469**, 543–547 (2011).
- 917 12. Roager, H. M. & Licht, T. R. Microbial tryptophan catabolites in health and disease. *Nat.*  
918 *Commun.* **9**, 3294 (2018).
- 919 13. Natividad, J. M. *et al.* Impaired Aryl Hydrocarbon Receptor Ligand Production by the Gut  
920 Microbiota Is a Key Factor in Metabolic Syndrome. *Cell Metab.* (2018).  
921 doi:10.1016/j.cmet.2018.07.001
- 922 14. Dodd, D. *et al.* A gut bacterial pathway metabolizes aromatic amino acids into nine  
923 circulating metabolites. *Nature* **551**, 648–652 (2017).
- 924 15. Guo, X. *et al.* Innate Lymphoid Cells Control Early Colonization Resistance against  
925 Intestinal Pathogens through ID2-Dependent Regulation of the Microbiota. *Immunity* **42**,  
926 731–743 (2015).
- 927 16. Zelante, T. *et al.* Tryptophan catabolites from microbiota engage aryl hydrocarbon receptor

- 928 and balance mucosal reactivity via interleukin-22. *Immunity* **39**, 372–385 (2013).
- 929 17. Hoyles, L. *et al.* Molecular phenomics and metagenomics of hepatic steatosis in non-diabetic  
930 obese women. *Nat. Med.* **24**, 1070–1080 (2018).
- 931 18. Krishnan, S. *et al.* Gut Microbiota-Derived Tryptophan Metabolites Modulate Inflammatory  
932 Response in Hepatocytes and Macrophages. *Cell Rep.* **23**, 1099–1111 (2018).
- 933 19. Madsen, A. L., Schack-Nielsen, L., Larnkjaer, A., Mølgaard, C. & Michaelsen, K. F.  
934 Determinants of blood glucose and insulin in healthy 9-month-old term Danish infants; the  
935 SKOT cohort. *Diabet. Med.* **27**, 1350–7 (2010).
- 936 20. Kato, K. *et al.* Age-Related Changes in the Composition of Gut Bifidobacterium Species.  
937 *Curr. Microbiol.* **74**, 987–995 (2017).
- 938 21. Koga, Y. *et al.* Age-associated effect of kestose on *Faecalibacterium prausnitzii* and  
939 symptoms in the atopic dermatitis infants. *Pediatr. Res.* **80**, 844–851 (2016).
- 940 22. Li, X., Jiang, B., Pan, B., Mu, W. & Zhang, T. Purification and partial characterization of  
941 *Lactobacillus* species SK007 lactate dehydrogenase (LDH) catalyzing phenylpyruvic acid  
942 (PPA) conversion into phenyllactic acid (PLA). *J. Agric. Food Chem.* **56**, 2392–2399 (2008).
- 943 23. Koide, S., Iwata, S., Matsuzawa, H. & Ohta, T. Crystallization of allosteric L-lactate  
944 dehydrogenase from *Thermus caldophilus* and preliminary crystallographic data. *J. Biochem.*  
945 **109**, 6–7 (1991).
- 946 24. Takashi, M., So, I., Hiroshi, S., Haruhiko, M. & Takahisa, O. Sequence and characteristics of  
947 the *Bifidobacterium longum* gene encoding l-lactate dehydrogenase and the primary structure  
948 of the enzyme: a new feature of the allosteric site. *Gene* **85**, 161–168 (1989).
- 949 25. Bottacini, F. *et al.* Global transcriptional landscape and promoter mapping of the gut  
950 commensal *Bifidobacterium breve* UCC2003. *BMC Genomics* **18**, 991 (2017).
- 951 26. Hirayama, Y. *et al.* Development of a double-crossover markerless gene deletion system in  
952 *Bifidobacterium longum*: Functional analysis of the ??-galactosidase gene for raffinose  
953 assimilation. *Appl. Environ. Microbiol.* **78**, 4984–4994 (2012).
- 954 27. Matsumura, H., Takeuchi, A. & Kano, Y. Construction of *Escherichia coli*-*Bifidobacterium*  
955 *longum* shuttle vector transforming *B. longum* 105-A and 108-A. *Biosci. Biotechnol.*  
956 *Biochem.* **61**, 1211–2 (1997).
- 957 28. Bakdash, J. Z. & Marusich, L. R. Repeated Measures Correlation. *Front. Psychol.* **8**, 456  
958 (2017).
- 959 29. Kim, S. ppcor: An R Package for a Fast Calculation to Semi-partial Correlation Coefficients.  
960 *Commun. Stat. Appl. methods* **22**, 665–674 (2015).
- 961 30. Alfa, M. J. *et al.* An Outbreak of Necrotizing Enterocolitis Associated with a Novel  
962 *Clostridium* Species in a Neonatal Intensive Care Unit. *Clin. Infect. Dis.* **35**, S101–S105  
963 (2002).

- 964 31. Butel, M.-J. *et al.* Conditions of Bifidobacterial Colonization in Preterm Infants: A  
965 Prospective Analysis. *J. Pediatr. Gastroenterol. Nutr.* **44**, (2007).
- 966 32. Moles, L. *et al.* Bacterial Diversity in Meconium of Preterm Neonates and Evolution of Their  
967 Fecal Microbiota during the First Month of Life. *PLoS One* **8**, e66986 (2013).
- 968 33. Arboleya, S. *et al.* Establishment and development of intestinal microbiota in preterm  
969 neonates. *FEMS Microbiol. Ecol.* **79**, 763–772 (2012).
- 970 34. Korpela, K. *et al.* Intestinal microbiota development and gestational age in preterm neonates.  
971 *Sci. Rep.* **8**, 2453 (2018).
- 972 35. Cervantes-Barragan, L. *et al.* Lactobacillus reuteri induces gut intraepithelial  
973 CD4(+)CD8 $\alpha\alpha$ (+) T cells. *Science* eaah5825 (2017). doi:10.1126/science.aah5825
- 974 36. Tamburini, S., Shen, N., Wu, H. C. & Clemente, J. C. The microbiome in early life:  
975 implications for health outcomes. *Nat. Med.* **22**, 713–722 (2016).
- 976 37. Dominguez-Bello, M. G., Godoy-Vitorino, F., Knight, R. & Blaser, M. J. Role of the  
977 microbiome in human development. *Gut* **68**, 1108–1114 (2019).
- 978 38. Sakurai, T., Odamaki, T. & Xiao, J.-Z. Production of Indole-3-Lactic Acid by  
979 Bifidobacterium Strains Isolated from Human Infants. *Microorganisms* **7**, 340 (2019).
- 980 39. Yamada, C. *et al.* Molecular Insight into Evolution of Symbiosis between Breast-Fed Infants  
981 and a Member of the Human Gut Microbiome Bifidobacterium longum. *Cell Chem. Biol.* **24**,  
982 515-524.e5 (2017).
- 983 40. Katayama, T. Host-derived glycans serve as selected nutrients for the gut microbe: human  
984 milk oligosaccharides and bifidobacteria. *Biosci. Biotechnol. Biochem.* **80**, 621–632 (2016).
- 985 41. Thomson, P., Medina, D. A. & Garrido, D. Human milk oligosaccharides and infant gut  
986 bifidobacteria: Molecular strategies for their utilization. *Food Microbiol.* **75**, 37–46 (2018).
- 987 42. Sakanaka, M. *et al.* Evolutionary adaptation in fucosyllactose uptake systems supports  
988 bifidobacteria-infant symbiosis. *Sci. Adv.* **5**, eaaw7696 (2019).
- 989 43. Vatanen, T. *et al.* The human gut microbiome in early-onset type 1 diabetes from the  
990 TEDDY study. *Nature* **562**, 589–594 (2018).
- 991 44. Natividad, J. M. *et al.* Impaired Aryl Hydrocarbon Receptor Ligand Production by the Gut  
992 Microbiota Is a Key Factor in Metabolic Syndrome. *Cell Metab.* **28**, 737-749.e4 (2018).
- 993 45. Metidji, A. *et al.* The Environmental Sensor AHR Protects from Inflammatory Damage by  
994 Maintaining Intestinal Stem Cell Homeostasis and Barrier Integrity. *Immunity* **49**, 353-362.e5  
995 (2018).
- 996 46. Gomez de Agüero, M. *et al.* The maternal microbiota drives early postnatal innate immune  
997 development. *Science (80-. )*. **351**, 1296–1302 (2016).
- 998 47. Kiss, E. A. *et al.* Natural Aryl Hydrocarbon Receptor Ligands Control Organogenesis of

- 999 Intestinal Lymphoid Follicles. *Science* (80-. ). **334**, 1561–1565 (2011).
- 1000 48. Qiu, J. *et al.* The Aryl Hydrocarbon Receptor Regulates Gut Immunity through Modulation  
1001 of Innate Lymphoid Cells. *Immunity* **36**, 92–104 (2012).
- 1002 49. Lamas, B. *et al.* CARD9 impacts colitis by altering gut microbiota metabolism of tryptophan  
1003 into aryl hydrocarbon receptor ligands. *Nat. Med.* (2016). doi:10.1038/nm.4102
- 1004 50. Hubbard, T. D. *et al.* Adaptation of the human aryl hydrocarbon receptor to sense  
1005 microbiota-derived indoles. *Sci. Rep.* **5**, 12689 (2015).
- 1006 51. Artis, D. & Spits, H. The biology of innate lymphoid cells. *Nature* **517**, 293–301 (2015).
- 1007 52. Dant, T. A. *et al.* T-cell expression of AhR inhibits the maintenance of pT<sub>reg</sub> cells in the  
1008 gastrointestinal tract in acute GVHD. *Blood* **130**, 348–359 (2017).
- 1009 53. Wilck, N. *et al.* Salt-responsive gut commensal modulates TH17 axis and disease. *Nature*  
1010 **551**, 585–589 (2017).
- 1011 54. Quintana, F. J. *et al.* Control of T(reg) and T(H)17 cell differentiation by the aryl  
1012 hydrocarbon receptor. *Nature* **453**, 65–71 (2008).
- 1013 55. Ning, Y. *et al.* Antibacterial activity of phenyllactic acid against *Listeria monocytogenes* and  
1014 *Escherichia coli* by dual mechanisms. *Food Chem.* **228**, 533–540 (2017).
- 1015 56. Rodríguez, N., Salgado, J. M., Cortés, S. & Domínguez, J. M. Antimicrobial activity of d-3-  
1016 phenyllactic acid produced by fed-batch process against *Salmonella enterica*. *Food Control*  
1017 **25**, 274–284 (2012).
- 1018 57. Narayanan, T. K. & Rao, G. R. Beta-indoleethanol and beta-indolelactic acid production by  
1019 *Candida* species: their antibacterial and autoantibiotic action. *Antimicrob. Agents Chemother.*  
1020 **9**, 375–80 (1976).
- 1021 58. Honoré, A. H. *et al.* Metabolic footprinting for investigation of antifungal properties of  
1022 *Lactobacillus paracasei*. *Anal. Bioanal. Chem.* **408**, 83–96 (2016).
- 1023 59. Peters, A. *et al.* Metabolites of lactic acid bacteria present in fermented foods are highly  
1024 potent agonists of human hydroxycarboxylic acid receptor 3. *PLOS Genet.* **15**, e1008145  
1025 (2019).
- 1026 60. Offermanns, S. Hydroxy-Carboxylic Acid Receptor Actions in Metabolism. *Trends*  
1027 *Endocrinol. Metab.* **28**, 227–236 (2017).
- 1028 61. Ahmed, K. *et al.* Deorphanization of GPR109B as a Receptor for the  $\beta$ -Oxidation  
1029 Intermediate 3-OH-octanoic Acid and Its Role in the Regulation of Lipolysis. *J. Biol. Chem.*  
1030 **284**, 21928–21933 (2009).
- 1031 62. Irukayama-Tomobe, Y. *et al.* Aromatic D-amino acids act as chemoattractant factors for  
1032 human leukocytes through a G protein-coupled receptor, GPR109B. *Proc. Natl. Acad. Sci.*  
1033 **106**, 3930–3934 (2009).

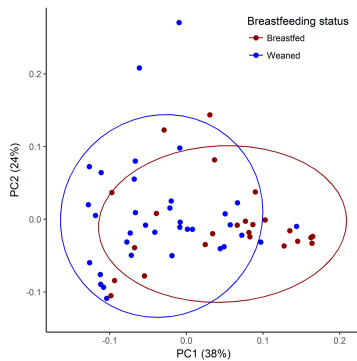
- 1034 63. Madsen, A. L., Larnkjær, A., Mølgaard, C. & Michaelsen, K. F. IGF-I and IGFBP-3 in  
1035 healthy 9 month old infants from the SKOT cohort: Breastfeeding, diet, and later obesity.  
1036 *Growth Horm. IGF Res.* **21**, 199–204 (2011).
- 1037 64. Laursen, M. F. *et al.* Having older siblings is associated with gut microbiota development  
1038 during early childhood. *BMC Microbiol.* **15**, 154 (2015).
- 1039 65. Laursen, M. F., Dalgaard, M. D. & Bahl, M. I. Genomic GC-Content Affects the Accuracy of  
1040 16S rRNA Gene Sequencing Based Microbial Profiling due to PCR Bias. *Front. Microbiol.*  
1041 **8**, 1934 (2017).
- 1042 66. Laursen, M. F. *et al.* Administration of two probiotic strains during early childhood does not  
1043 affect the endogenous gut microbiota composition despite probiotic proliferation. *BMC*  
1044 *Microbiol.* **17**, 175 (2017).
- 1045 67. Edgar, R. C. UPARSE: highly accurate OTU sequences from microbial amplicon reads. *Nat.*  
1046 *Methods* **10**, 996–8 (2013).
- 1047 68. Caporaso, J. G. *et al.* QIIME allows analysis of high-throughput community sequencing data.  
1048 *Nat. Methods* **7**, 335–6 (2010).
- 1049 69. Wang, Q., Garrity, G. M., Tiedje, J. M. & Cole, J. R. Naive Bayesian classifier for rapid  
1050 assignment of rRNA sequences into the new bacterial taxonomy. *Appl. Environ. Microbiol.*  
1051 **73**, 5261–7 (2007).
- 1052 70. DeSantis, T. Z. *et al.* Greengenes, a chimera-checked 16S rRNA gene database and  
1053 workbench compatible with ARB. *Appl. Environ. Microbiol.* **72**, 5069–72 (2006).
- 1054 71. Altschul, S. F., Gish, W., Miller, W., Myers, E. W. & Lipman, D. J. Basic local alignment  
1055 search tool. *J. Mol. Biol.* **215**, 403–410 (1990).
- 1056 72. Frese, S. A. *et al.* Persistence of Supplemented *Bifidobacterium longum* subsp. *infantis*  
1057 EVC001 in Breastfed Infants. (2017). doi:10.1128/mSphere
- 1058 73. Lawley, B. *et al.* Differentiation of *Bifidobacterium longum* subspecies *longum* and *infantis*  
1059 by quantitative PCR using functional gene targets. *PeerJ* **5**, e3375 (2017).
- 1060 74. Sprenger, N., Lee, L. Y., De Castro, C. A., Steenhout, P. & Thakkar, S. K. Longitudinal  
1061 change of selected human milk oligosaccharides and association to infants' growth, an  
1062 observatory, single center, longitudinal cohort study. *PLoS One* **12**, e0171814 (2017).
- 1063 75. Xu, G. *et al.* Absolute Quantitation of Human Milk Oligosaccharides Reveals Phenotypic  
1064 Variations during Lactation. *J. Nutr.* **147**, 117–124 (2017).
- 1065 76. Sakurama, H. *et al.* Lacto-N-biosidase encoded by a novel gene of *bifidobacterium longum*  
1066 subspecies *longum* shows unique substrate specificity and requires a designated chaperone  
1067 for its active expression. *J. Biol. Chem.* **288**, 25194–25206 (2013).
- 1068 77. Sakanaka, M. *et al.* Functional analysis of bifidobacterial promoters in *Bifidobacterium*  
1069 *longum* and *Escherichia coli* using the  $\alpha$ -galactosidase gene as a reporter. *J. Biosci. Bioeng.*



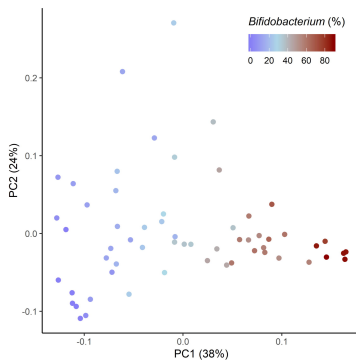
- 1070 **118**, 489–495 (2014).
- 1071 78. Poolman, B., Nijssen, R. M. J. & Konings, W. N. Dependence of *Streptococcus lactis*  
1072 phosphate transport on internal phosphate concentration and internal pH. *J. Bacteriol.* **169**,  
1073 5373–5378 (1987).
- 1074 79. Barri, T., Holmer-Jensen, J., Hermansen, K. & Dragsted, L. O. Metabolic fingerprinting of  
1075 high-fat plasma samples processed by centrifugation- and filtration-based protein  
1076 precipitation delineates significant differences in metabolite information coverage. *Anal.*  
1077 *Chim. Acta* **718**, 47–57 (2012).
- 1078 80. Nielsen, L. N. *et al.* Glyphosate has limited short-term effects on commensal bacterial  
1079 community composition in the gut environment due to sufficient aromatic amino acid levels.  
1080 *Environ. Pollut.* **233**, (2018).
- 1081 81. Roager, H. M. *et al.* Colonic transit time is related to bacterial metabolism and mucosal  
1082 turnover in the gut. *Nat. Microbiol.* **1**, 16093 (2016).
- 1083 82. Smith, C. A., Want, E. J., O’Maille, G., Abagyan, R. & Siuzdak, G. XCMS: Processing Mass  
1084 Spectrometry Data for Metabolite Profiling Using Nonlinear Peak Alignment, Matching, and  
1085 Identification. *Anal. Chem.* **78**, 779–787 (2006).
- 1086 83. Sumner, L. W. *et al.* Proposed minimum reporting standards for chemical analysis Chemical  
1087 Analysis Working Group (CAWG) Metabolomics Standards Initiative (MSI). *Metabolomics*  
1088 **3**, 211–221 (2007).
- 1089 84. Gürdeniz, G., Kristensen, M., Skov, T. & Dragsted, L. O. The Effect of LC-MS Data  
1090 Preprocessing Methods on the Selection of Plasma Biomarkers in Fed vs. Fasted Rats.  
1091 *Metabolites* **2**, 77–99 (2012).
- 1092 85. Pluskal, T., Castillo, S., Villar-Briones, A. & Oresic, M. MZmine 2: modular framework for  
1093 processing, visualizing, and analyzing mass spectrometry-based molecular profile data. *BMC*  
1094 *Bioinformatics* **11**, 395 (2010).
- 1095 86. van der Kloet, F. M., Bobeldijk, I., Verheij, E. R. & Jellema, R. H. Analytical error reduction  
1096 using single point calibration for accurate and precise metabolomic phenotyping. *J. Proteome*  
1097 *Res.* **8**, 5132–41 (2009).
- 1098 87. Smart, K. F., Aggio, R. B. M., Houtte, J. V. R. Van & Villas-Bôas, S. G. Analytical platform  
1099 for metabolome analysis of microbial cells using methyl chloroformate derivatization  
1100 followed by gas chromatography-mass spectrometry. *Nat. Protoc.* **5**, 1709–1729 (2010).
- 1101 88. Johnsen, L. G., Skou, P. B., Khakimov, B. & Bro, R. Gas chromatography – mass  
1102 spectrometry data processing made easy. *J. Chromatogr. A* **1503**, 57–64 (2017).
- 1103 89. Rosenmai, A. K. *et al.* Are structural analogues to bisphenol a safe alternatives? *Toxicol. Sci.*  
1104 **139**, 35–47 (2014).
- 1105 90. R Core Team. R: A language and environment for statistical computing. (2013).

- 1106 91. Wickham, H. *ggplot2 Elegant Graphics for Data Analysis*. (Springer, New York, 2009).
- 1107 92. Vu, V. *ggbiplot: a ggplot2 based biplot*. 2011
- 1108 93. Warnes, G. R. *et al.* *gplots: Various R Programming Tools for Plotting Data*. R package  
1109 version 2.16.0. *CRAN* (2015).
- 1110 94. Benjamini, Y. & Hochberg, Y. Controlling the False Discovery Rate - a Practical and  
1111 Powerful Approach to Multiple Testing. *J. R. Stat. Soc. Ser. B-Methodological* **57**, 289–300  
1112 (1995).
- 1113 95. Smith, E. A. & Macfarlane, G. T. Enumeration of human colonic bacteria producing phenolic  
1114 and indolic compounds: effects of pH, carbohydrate availability and retention time on  
1115 dissimilatory aromatic amino acid metabolism. *J. Appl. Bacteriol.* **81**, 288–302 (1996).
- 1116 96. Smith, E. A. & Macfarlane, G. T. Formation of Phenolic and Indolic Compounds by  
1117 Anaerobic Bacteria in the Human Large Intestine. *Microb. Ecol.* **33**, 180–188 (1997).

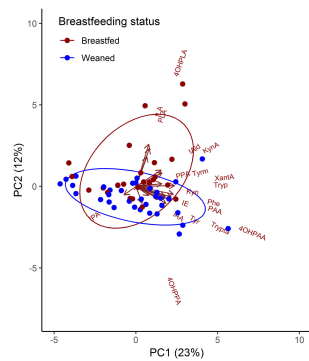
a



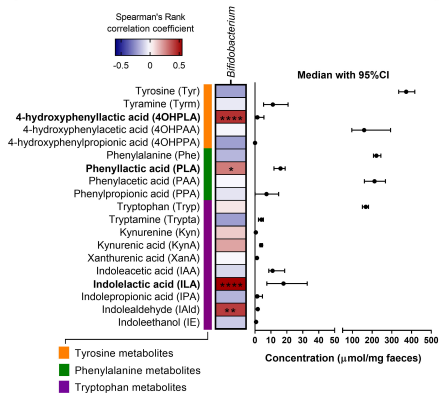
b



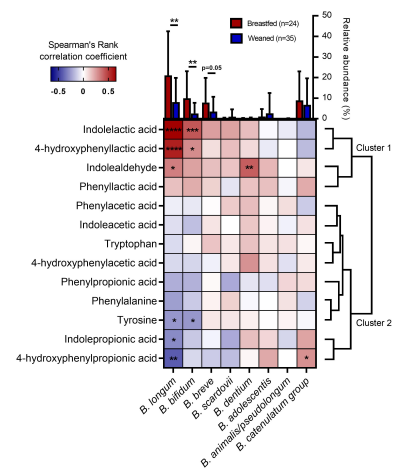
c



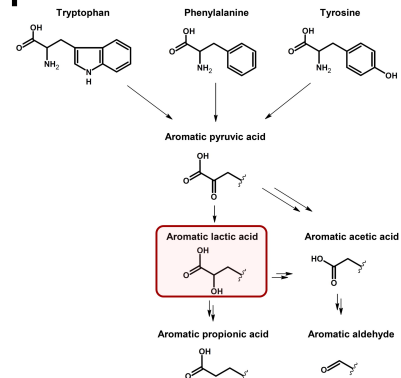
d

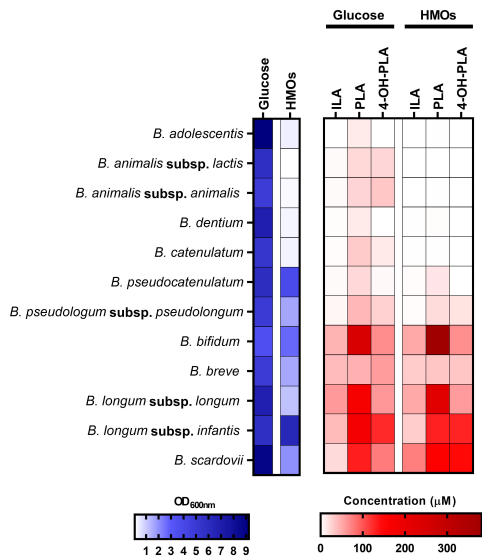
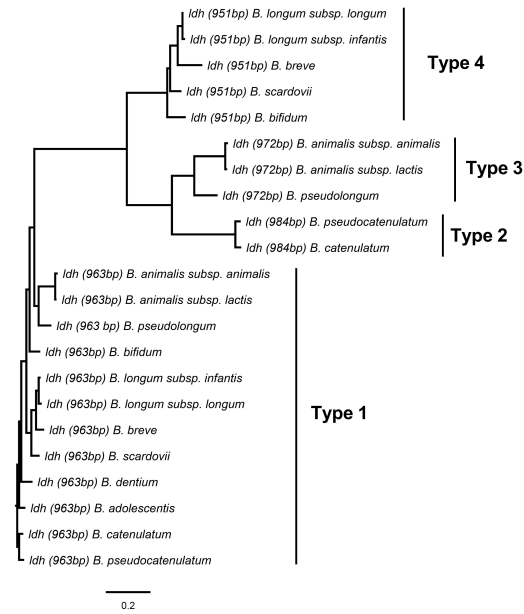
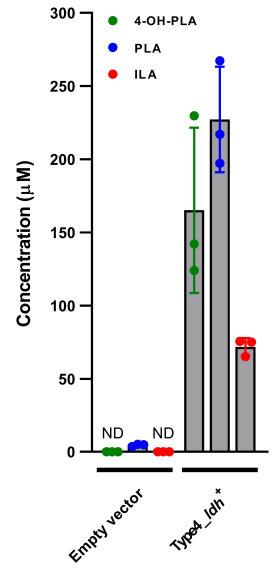
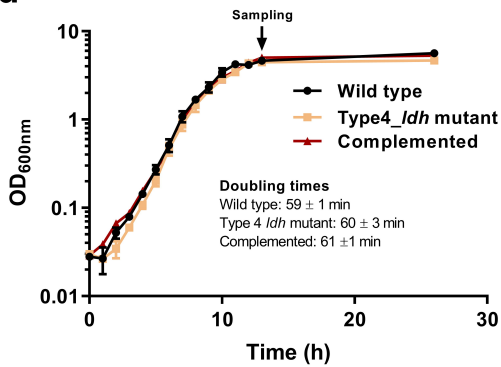
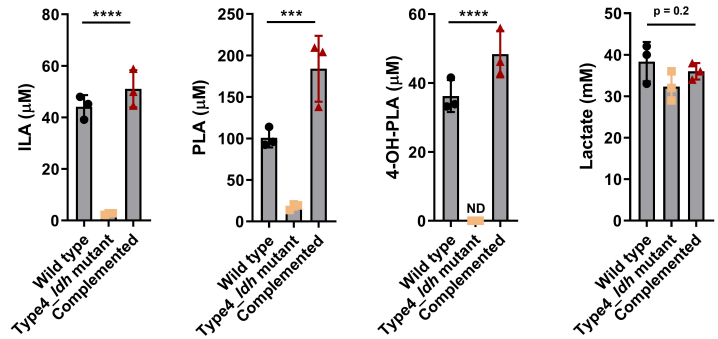
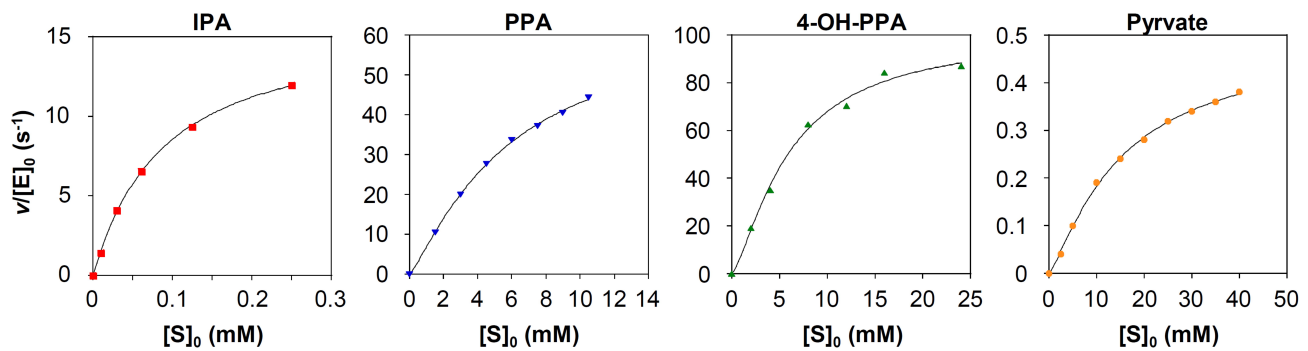


e



f



**a****b****c****d****e****f****g**

Kinetic parameters (Hill equation) of type 4 LDH

Substrate	$K_{0.5}$ (mM)	$k_{\text{cat}}$ ( $\text{s}^{-1}$ )	$k_{\text{cat}}/K_{0.5}$ ( $\text{s}^{-1} \text{mM}^{-1}$ )	$n_H$ (Hill coefficient)
IPA	$0.08 \pm 0.01$	$15.21 \pm 1.01$	193.73	$1.05 \pm 0.02$
PPA	$5.96 \pm 0.06$	$64.22 \pm 2.38$	10.77	$1.20 \pm 0.01$
4-OH-PPA	$6.61 \pm 0.93$	$103.89 \pm 4.32$	15.83	$1.39 \pm 0.01$
Pyruvate	$14.88 \pm 0.48$	$0.47 \pm 0.03$	0.03	$1.28 \pm 0.05$

